THE JOURNAL OF PHYSICAL CHEMISTRY A
A JOURNAL OF THE AMERICAN CHEMICAL SOCIETY

pubs.acs.org/JPCA Article

First-Principles Prediction for Phosphorescence Spectra of Tetradentate Platinum(II) Complexes with Narrow Emission Width

Xiao Chen, Shanhao Deng, Wenjie Zhang, Pingan Yin, Weitang Li, and Zhigang Shuai*

Cite This: J. Phys. Chem. A 2025, 129, 2493−2509 Read Online

ACCESS | Metrics & More | Article Recommendations | Supporting Information

ABSTRACT: Heavy metal complexes are important organic light-emitting diode (OLED) materials, with the advantage of theoretically up to 100% quantum efficiency, but suffer from low color purity, specifically due to a large emission spectral width. Recently, several tetradentate platinum(II) complexes have been found to demonstrate a narrow emission width. In order to suggest a molecular design strategy to achieve narrow emission width, we combine density functional theory (DFT) and its time-dependent formalism coupled with the thermal vibrational correlation function (TVCF) formalism to evaluate the emission energy and spectral line shape for 50 tetradentate platinum(II) complex compounds. We have benchmarked the computational approach by testing 14 xc-functionals and 4 potential energy surface models. We find that the pyridine-carbazole-oxygen structure is the essential moiety to achieve high color purity for the Pt(II) coordination compounds, which can suppress the excitation of low-frequency vibrational relaxation motion during phosphorescence emission, leading to a narrow emission spectrum.

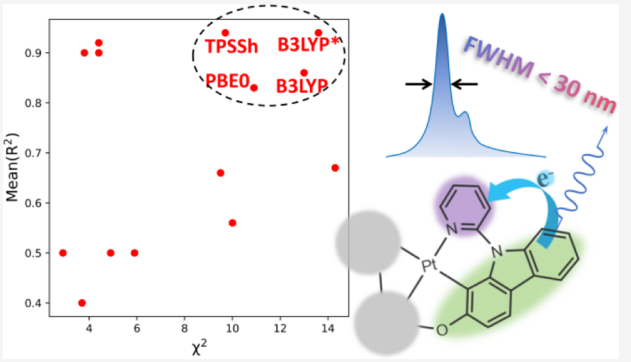

1. INTRODUCTION

Organic light-emitting diode (OLED) materials have become integrated into modern industry due to their exceptional display and lighting properties. Organometallic molecules, particularly those incorporating heavy metals such as platinum and iridium, have been extensively utilized in the second-generation phosphorescent OLED materials.[1] The efficient intersystem crossing (ISC) process in these materials enables the conversion of electrically excited carriers into triplet (T_1) states, facilitating phosphorescence with a theoretical luminescence efficiency approaching 100%. This advancement has allowed phosphorescent materials to surpass the low internal quantum efficiency of first-generation fluorescent OLEDs, thereby shifting the focus toward blue emitting and color purity as critical performance indicators. Researchers have explored a diversity of coordination groups and substituents, synthesizing numerous phosphorescent molecules emitting across various colors.[2−26] It was found that the Pt(II) coordinated compound can emit blue light. However, these molecules exhibit low color purity, primarily due to significant structural relaxation from the T_1 state to the ground state (S_0).[27−29] Despite several theoretical studies aimed at addressing these challenges,[30−37] a systematic approach to enhancing the color purity of their emission spectra remains elusive.

In 2014, the tetradentate platinum(II) complexes PtON7 and PtON7-dtb were synthesized, representing significant advancements in blue phosphorescent materials.[38] These molecules not only exhibited external quantum efficiencies (EQEs) exceeding 20%, but also PtON7-dtb demonstrated high color purity, characterized by an emission spectrum with a full width at half-maximum (FWHM) of merely 20 nm. This work underscored the potential of tetradentate platinum complexes as superior candidates of materials with high color purity, and then a series of compounds with analogous structures were synthesized and characterized.[39] In 2022, another two blue molecules, BD-01 and BD-02, were synthesized, which not only maintained high color purity and EQE but also exhibited device lifetimes exceeding 1000 h.[40] The consistent narrowband emission properties observed in these structurally similar molecules suggest a strong correlation between the high color purity and their tetradentate configurations. Theoretical elucidation of this relationship is imperative as it would significantly enhance the rational design of new molecules and devices with optimized performance.

To analyze the relationship between the structure and emission color purity of organic materials, it is essential to develop efficient theoretical methods that accurately capture the effects of vibrational properties on emission spectra. The

Received: December 14, 2024
Revised: February 14, 2025
Accepted: February 20, 2025
Published: March 1, 2025

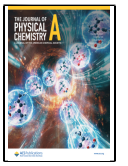

https://doi.org/10.1021/acs.jpca.4c08452
J. Phys. Chem. A 2025, 129, 2493−2509

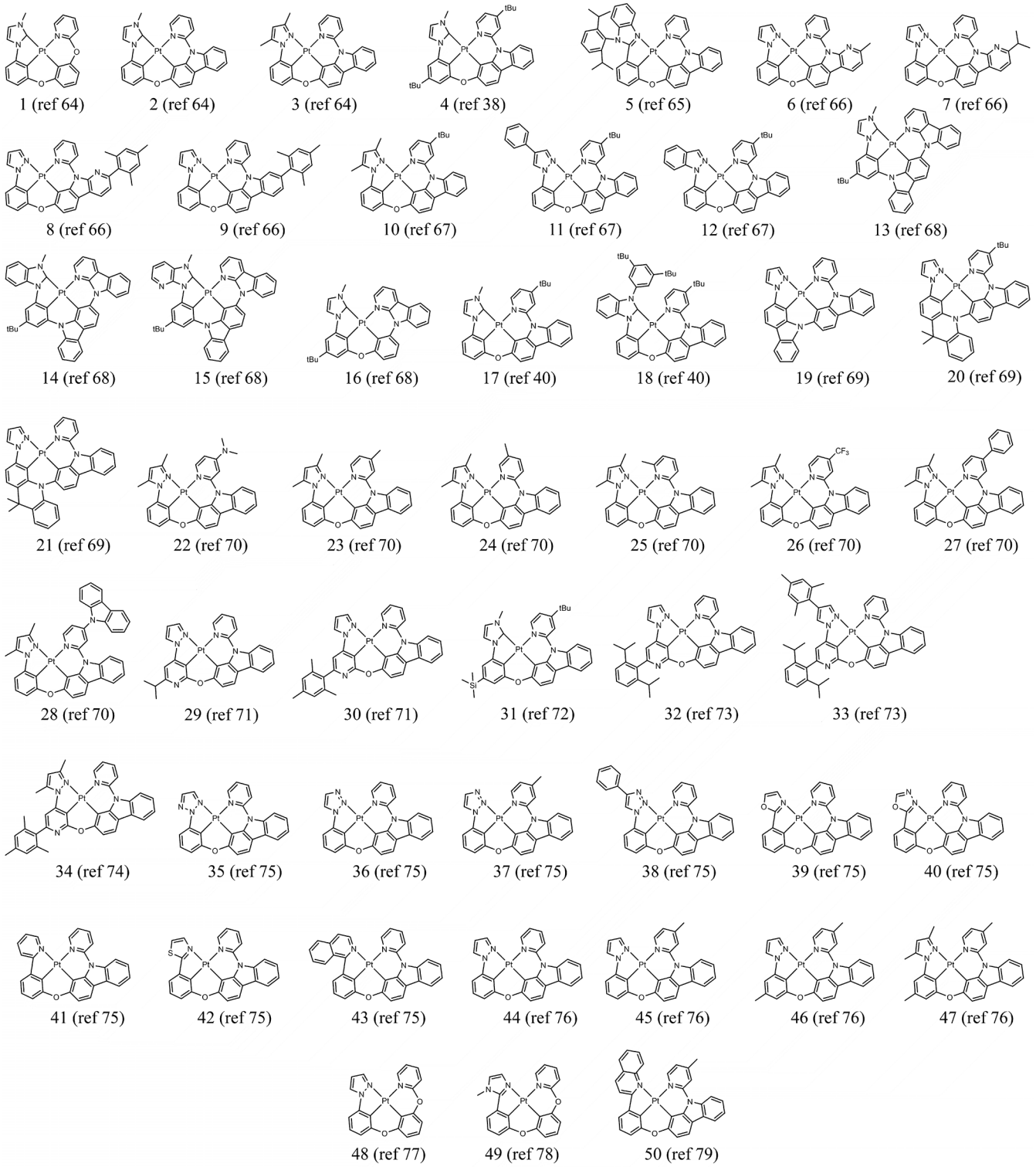

Figure 1. Structures of the molecules studied in this work.

formulations for the vibrationally resolved emission spectra have been derived in detail by Strickler and Berg.[41,42] Moreover, utilizing the thermal vibration correlation function (TVCF) method enables these calculations to be performed efficiently.[43−50] In a previous work by our group, we revealed the characteristics of the deactivation process in these platinum molecules, showing that direct vibrational relaxation is their main nonradiative deactivation channel, while the minimum energy crossing points are usually unimportant, which partly explains the higher luminescence efficiency of tetradentate platinum complexes.[51] This method is also widely employed in studies of radiative and nonradiative processes in other systems.[52−54]

However, two essential prerequisites must be met to accurately employ the TVCF method for these tetradentate platinum compounds. First, the electronic information is required, including the equilibrium geometries and vibrational frequencies of the initial and final electronic states. Although the

https://doi.org/10.1021/acs.jpca.4c08452
J. Phys. Chem. A 2025, 129, 2493−2509

density functional theory (DFT) and time-dependent density functional theory (TD-DFT) may provide these data efficiently, it is well known that the accuracy of these calculations is significantly influenced by the choice of the functional.[55−59] Thus, identifying a suitable functional for these systems is of paramount importance. Second, a proper model for the potential energy surface is required, which relates the vibronic wave functions of the two states. The model constructed using Cartesian coordinates is widely employed, while that constructed by internal coordinates sometimes gives more reliable results for flexible molecules.[60−63] Furthermore, the consideration of vibrational mode mixing—also known as the Duschinsky rotation effect (DRE)—can introduce additional differences in the results.[54]

In this study, we investigate the performance of 14 functionals in predicting the photophysical properties of 50 tetradentate platinum(II) complexes. By comparing the computed emission energies and spectral shapes with experimental data, we identified the functionals that provide the best agreement. Meanwhile, the results of different potential energy surface models are compared. We then analyze the vibronic properties and electronic transition characteristics of molecules exhibiting either narrow or broad emission bandwidths. Our analysis reveals that the presence of a pyridine-carbazole-oxygen moiety is a critical factor in achieving high color purity. For molecules lacking this moiety, numerous low-frequency vibrational modes are activated during the T_1-S_0 transition, leading to the broadening of the emission peak. In contrast, for molecules containing this moiety, especially those with no other structure significantly conjugated to it, only two high-frequency modes are slightly activated, thus maintaining a high color purity of phosphorescence emission. Our work elucidates the structure−property relationships of tetradentate platinum(II) complexes and provides theoretical support for the efficient screening and design of new molecules with superior photophysical properties.

2. METHODOLOGY

The 50 tetradentate platinum(II) complexes examined in this study are all previously reported compounds; their molecular structures and corresponding literature sources are depicted in Figure 1. The relevant experimental data, including the peak emission energies and FWHM of their phosphorescence spectra, are summarized in Table S2. Here, only the main emission peak for each molecule is considered, ignoring all possibly existing shoulders. All experimental data are taken from dilute solutions of dichloromethane (DCM) at room temperature, which facilitates the systematic calculation and enables a consistent comparison of results.

The functionals used in this paper include B3LYP,[80] ωB97X-D,[81] CAM-B3LYP,[82] MN15,[83] M06-2X,[84] TPSSh,[85,86] BMK,[87] BHHLYP,[88] B3LYP*,[89] PBE0,[90] PBE38,[91] PBE,[92] TPSS,[85] and BP86.[93,94] For each molecule and each functional, DFT and UDFT methods are employed, respectively, for optimization to get the S_0 structure and T_1 structure, followed by vibrational frequency calculation to confirm that a true minimum is reached. A TDDFT single-point energy calculation is conducted at the T_1 structure, while a UDFT single-point energy calculation is performed at the S_0 structure. All the above calculations are carried out using the Gaussian16[95] software package with the def2-svp[96,97] basis set. The polarizable continuum model (PCM) is used to introduce the DCM solvent environment.[98] Dispersion corrections are applied for all functionals except B3LYP*, with correction coefficients detailed in Table S1. Electronic structure analysis and charge density difference (CDD) data are provided by Multiwfn in combination with TDDFT data.[99,100]

Since the phosphorescence emission energy of a molecule is contributed by both electronic and vibrational components, to obtain its emission peak energy, one needs to consider both the electronic state energy gap and the vibrational energy difference with the largest Franck−Condon factor. However, usually, the electronic energy gap is dominant; thus, the adiabatic or vertical energy gap of the electronic states can usually be used as an approximation of the emission peak energy. The former is defined as the energy difference between the two electronic states at their respective equilibrium structures, whereas the latter refers to the energy difference between the two electronic states under the equilibrium structure of the initial state. Meanwhile, triplet state energies can be given by both UDFT and TDDFT methods, so that, in combination with the aforementioned adiabatic or vertical models, four different quantities can be generated to estimate the emission peak energy:

$$\begin{aligned} E_{\mathrm{v,td}} &= E_{\mathrm{t,td}} - E_{\mathrm{gt}} \\ E_{\mathrm{v,u}} &= E_{\mathrm{t,u}} - E_{\mathrm{gt}} \\ E_{\mathrm{ad,td}} &= E_{\mathrm{t,td}} - E_{\mathrm{g}} \\ E_{\mathrm{ad,u}} &= E_{\mathrm{t,u}} - E_{\mathrm{g}} \end{aligned} \tag{1}$$

Here, v, ad, u, and td denote vertical, adiabatic, UDFT, and TDDFT, respectively, g and gt denote the ground state energy in optimized S_0 or T_1 structure, and t denotes the T_1 state energy in optimized T_1 structure. Their physical meanings are listed in Figure 2. For each set of quantities, the statistics AVR (average),

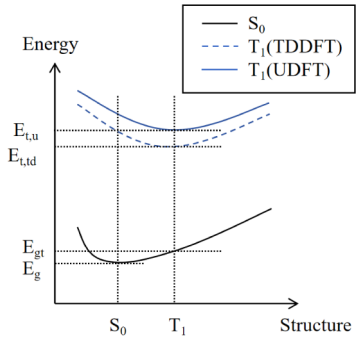

Figure 2. Annotation diagram of the potential energy surface.

RMSD (root mean squared error), and MAR (mean absolute residual) are given by

$$\begin{aligned} \mathrm{AVR} &= \frac{1}{N}\sum_{\mathrm{i}} (x_{\mathrm{i}} - y_{\mathrm{i}}) \\ \mathrm{RMSD} &= \sqrt{\sum_{\mathrm{i}} (x_{\mathrm{i}} - y_{\mathrm{i}})^2 / N} \\ \mathrm{MAR} &= \frac{1}{N}\sum_{\mathrm{i}} |y_{\mathrm{i}} - kx_{\mathrm{i}} - b| \end{aligned} \tag{2}$$

Here, x_{i} and y_{i} denote the calculated and the corresponding experimental values, respectively, while k and b are the regression coefficients given by the ordinary least-squares method.

https://doi.org/10.1021/acs.jpca.4c08452
J. Phys. Chem. A 2025, 129, 2493−2509

Table 1. AVR and RMSD of Emission Peak Energy between Computed and Experimental Data

pred. - exp. (eV) AVR/RMSD	$E_{v,td}$	$E_{v,u}$	$E_{ad,td}$	$E_{ad,u}$
CAM-B3LYP	−0.23/0.38	−0.13/0.19	0.22/0.37	0.32/0.33
TPSSh	−0.46/0.47	−0.29/0.30	−0.26/0.26	−0.09/0.11
BMK	−0.06/0.18	−0.14/0.20	0.33/0.38	0.25/0.26
ωB97X-D	−0.13/0.33	−0.08/0.15	0.32/0.44	0.37/0.38
PBE0	−0.34/0.39	−0.21/0.27	−0.02/0.12	0.11/0.12
M06-2X	0.09/0.29	0.05/0.21	0.56/0.61	0.52/0.52
PBE38	−0.35/0.44	−0.19/0.24	0.07/0.29	0.23/0.24
TPSS	−0.66/0.66	−0.43/0.43	−0.51/0.51	−0.27/0.28
PBE	−0.71/0.72	−0.45/0.46	−0.58/0.58	−0.32/0.33
B3LYP*	−0.39/0.40	−0.24/0.24	−0.18/0.18	−0.02/0.06
BP86	−0.72/0.72	−0.46/0.46	−0.58/0.59	−0.32/0.33
MN15	−0.11/0.24	−0.04/0.10	0.26/0.33	0.33/0.34
BHHLYP	−0.53/0.66	−0.17/0.27	−0.01/0.40	0.35/0.37
B3LYP	−0.36/0.38	−0.23/0.24	−0.09/0.12	0.05/0.08

According to Fermi's golden rule (FGR), the spectral line shape $L(\omega)$ of spontaneous emission is given by

$$L(\omega) = \sum_{i,f} \omega^3 \rho_i(T) |\langle \psi_i | \vec{\mu} | \psi_f \rangle|^2 \delta\left(\omega_f - \omega_i - \frac{\Delta E_{ad}}{\hbar} + \omega\right) \tag{3}$$

where ρ, ψ, μ, and ΔE_{ad} denote, respectively, the Boltzmann population, wave function, transition dipole operator, and the adiabatic energy gap, and i and f run over all initial and final vibrational states. Introducing the Franck−Condon (FC) approximation and the harmonic approximation, the above equation can be further transformed as

$$L(\omega) = \sum_{i,f} \omega^3 \rho_i(T) |\langle \Phi_{T_1} | \vec{\mu} | \Phi_{S_0} \rangle|^2 |\langle \Psi_i(\vec{Q}) | \Psi_f(\vec{Q}') \rangle|^2 \delta \left(\omega_f - \omega_i - \frac{\Delta E_{ad}}{\hbar} + \omega\right) \tag{4}$$

where Φ and Ψ denote the electronic and vibrational wave functions, respectively. Now the vibrational wave function is the product of a series of one-dimensional harmonic oscillator wave functions, whose variables, Q and Q', are linked by the linear Duschinsky relation

$$\vec{Q}' = J\vec{Q} + \vec{K} \tag{5}$$

with J the Duschinsky rotation matrix, and K the mode displacement. Calculations of J and K can be conducted using either Cartesian or internal coordinates, the former being straightforward but likely to fail when dealing with flexible molecules, that is, molecules with significantly different structures at initial and final states.[60−63] Since some of the molecules studied here have distinctly flexible structures, such as isopropyl and biphenyl, internal coordinates are used unless otherwise stated.

Full consideration of the linear Duschinsky relation is also called the Adiabatic Hessian (AH) model, among other popular potential energy surface models such as Vertical Hessian (VH), Adiabatic Shift (AS), Vertical Gradient (VG), and displaced harmonic oscillator with different frequencies (DODF).[54,63,101,107−109] In AH and VH models, the Hessian in the excited state may be different from that in the ground state, while in AS and VG models, the two Hessian matrices are approximately treated as the same—that is, taking J as an identity matrix. Besides, the AH and AS models perform optimization to find the exact equilibrium structure of the excited state. In contrast, the VH and VG models obtain the excited state equilibrium structure by extrapolation according to the gradient in the ground state structure. The DODF model is intermediate between AH and AS, allowing the two potential energy surfaces to have different shapes but ignoring the difference in orientation. All calculations in this study employ the AH model with a linear Duschinsky relation, except for the section specifically devoted to investigating the DRE.

Given the relation between the two sets of normal coordinates, there are two ways to derive the overlap integrals of the vibrational wave functions in $L(\omega)$. The time-independent method directly solves and sums the overlap integrals pairwise and is thus also known as the sum-of-states method. This method has been widely used, for example, in the calculation of absorption and emission spectra of several organic molecules.[110] However, since there are an infinite number of vibrational states, practical calculations need truncation, which can introduce errors.[101] Moreover, the computational effort of this method grows exponentially with the number of vibrational modes, making it unsuitable for large systems. The time-dependent method, also known as the thermal vibrational correlation function (TVCF) method, transforms $L(\omega)$ into a correlation function χ in the time domain via a Fourier transform. χ can be expressed using the partition function Z_{vib} and vibrational Hamiltonian H_i and H_f for the initial and final state, and it possesses a known analytical expression. Therefore, the TVCF method exhibits only polynomial complexity and does not introduce truncation errors. In this work, all spectra are calculated using the TVCF method, and the software package MOMAP[47−50] is used for these calculations, taking temperature T = 300 K.

$$L(\omega) = \frac{1}{2\pi} \int \omega^3 e^{-it(\Delta E_{ad}/\hbar - \omega)} \chi(t, T) dt$$

$$\chi(t, T) = Z_{vib}^{-1} Tr[e^{(i\hat{H}_i/\hbar - \beta \hat{H}_i)t} e^{-i\hat{H}_f t/\hbar}] \tag{6}$$

3. RESULTS AND DISCUSSION

3.1. Emission Peak. The calculated results for each functional applied to each molecule are presented in Table S4, with statistical analyses comparing these results to the corresponding experimental values summarized in Table 1. Across all functionals, $E_{v,td}$ consistently yields the lowest values, and $E_{ad,u}$ yields the highest, while the magnitudes of $E_{ad,td}$ and

https://doi.org/10.1021/acs.jpca.4c08452
J. Phys. Chem. A 2025, 129, 2493−2509

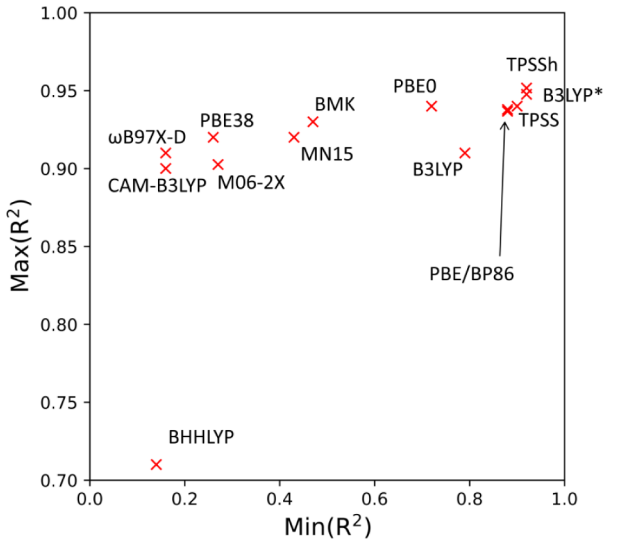

Figure 3. Maximum and minimum among the R^2 given by the 4 sets of quantities for each functional.

$E_{v,u}$ vary with the functional employed. The RMSD of the TDDFT results is generally larger than that of the corresponding UDFT results, suggesting that UDFT provides a better reflection of the trend in the phosphorescence emission energies, as will be demonstrated later. A comparison among the functionals reveals that the calculated emission energies increase roughly with the proportion of Hartree−Fock (HF) exchange included in the functional, with the pure functionals all significantly underestimating the emission energy. TPSSh (10% HF), B3LYP* (15% HF), and B3LYP (20% HF) give the smallest emission energies among the hybrid functionals, and those given by M06-2X (56% HF) are always the largest. Among all four sets of quantities of all the functionals, B3LYP*/$E_{ad,u}$ performs the best, followed by B3LYP/$E_{ad,u}$ and MN15/$E_{v,u}$, which all achieve AVR not exceeding ±0.05 eV and RMSD less than 0.10 eV.

To better illustrate the trend, scatter plots of the predicted emission wavelength against the experimental values are constructed (see Figure S1 for all plots). Since the errors have been discussed above, here, we focus on the degree of linearity between the computed and experimental values. The results show that 14 functionals can be roughly classified into two categories. The first category includes TPSSh, TPSS, PBE, B3LYP*, and BP86, which exhibit a high and roughly comparable degree of linearity between the four sets of calculated results and the experimental values (Figure 3).

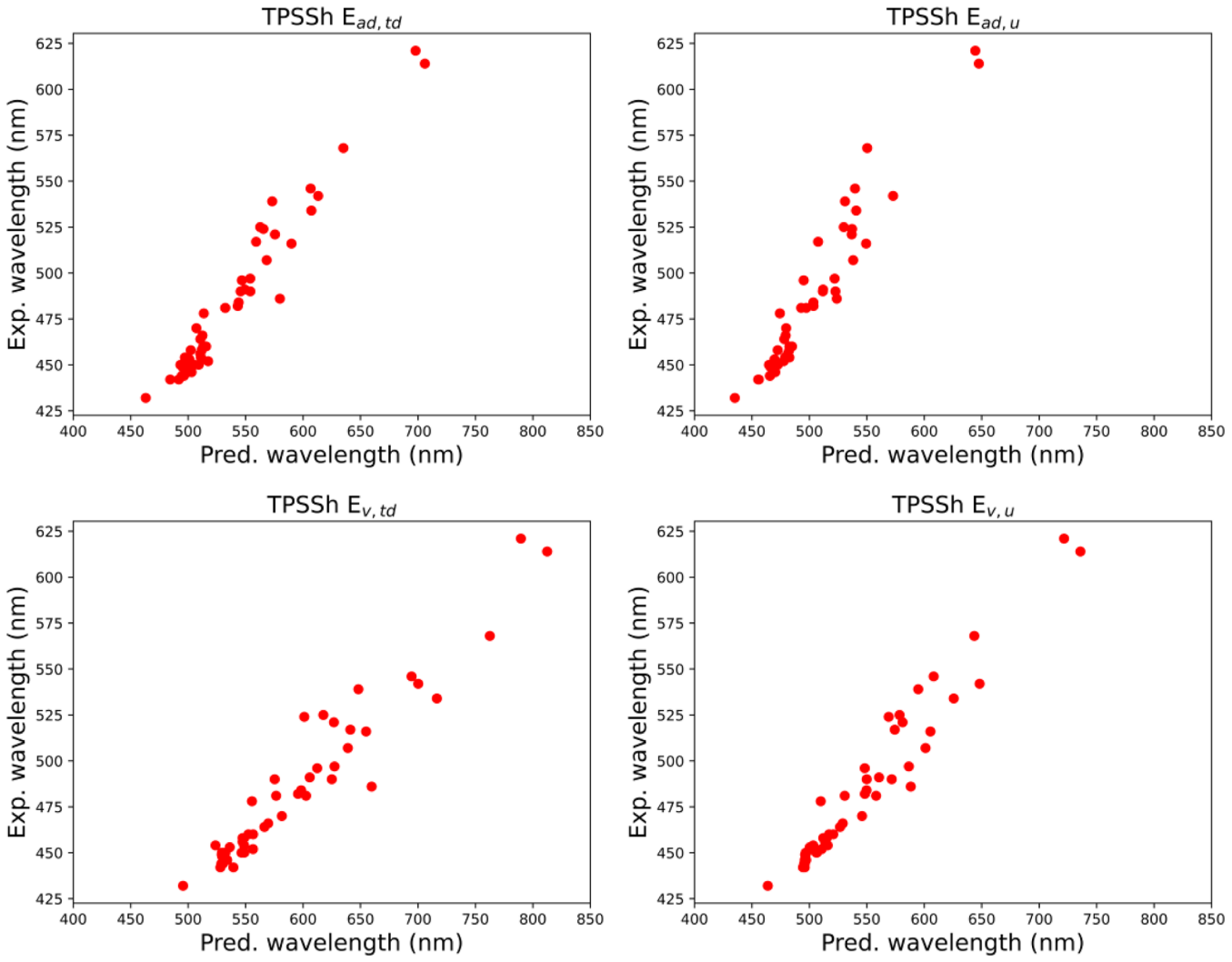

Figure 4. Scatter plots of TPSSh results of emission peak wavelengths against experimental values.

https://doi.org/10.1021/acs.jpca.4c08452
J. Phys. Chem. A 2025, 129, 2493−2509

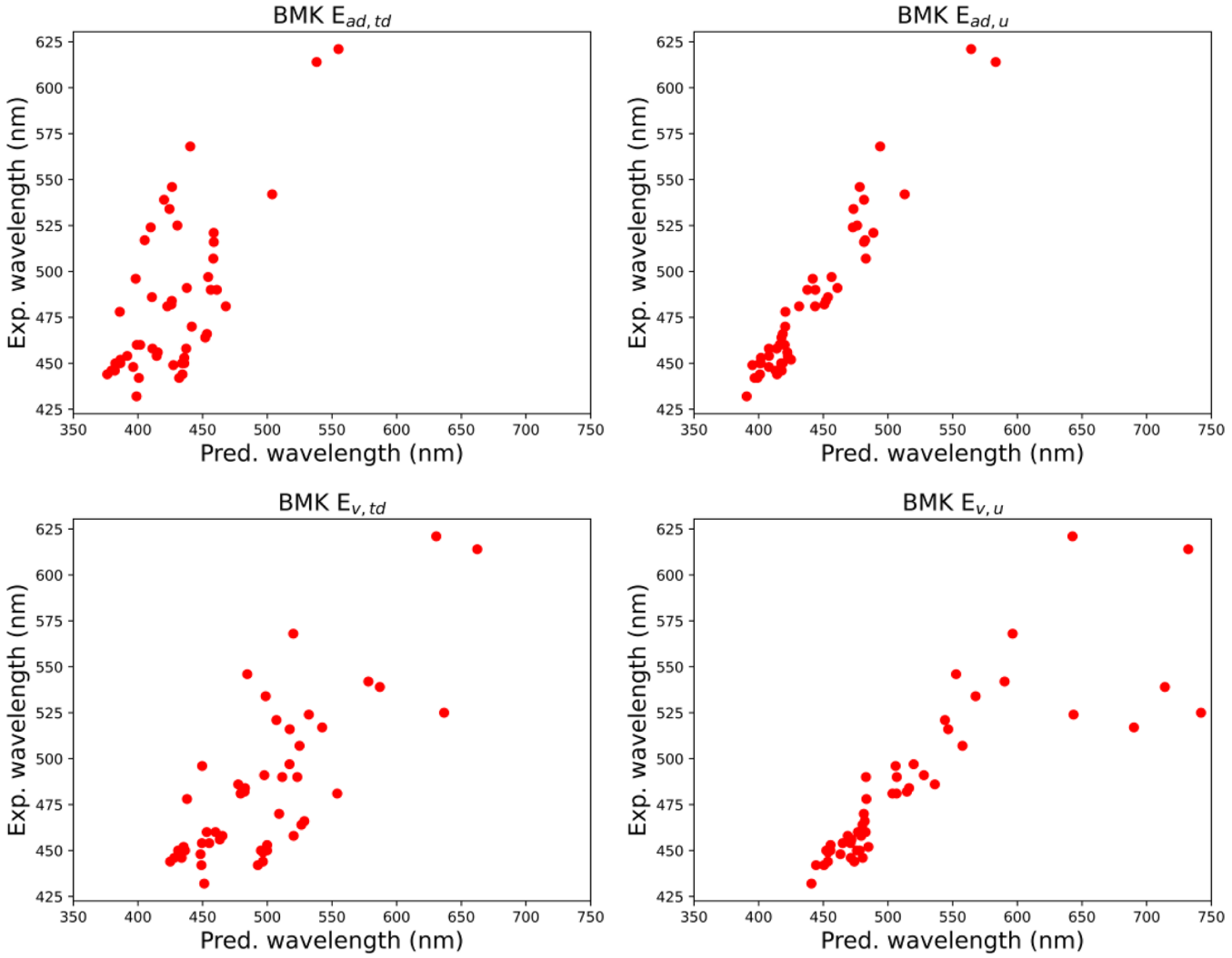

Figure 5. Scatter plots of BMK results of emission peak wavelengths against experimental values.

Table 2. R^2 between Predicted and Experimental Values for the Emission Peak Wavelengths. For those with $R^2 > 0.9$, Corresponding MAR are also given

exp. ~ pred. R^2/MAR (nm)	$E_{v,td}$	$E_{v,u}$	$E_{ad,td}$	$E_{ad,u}$
CAM-B3LYP	0.19	0.74	0.16	0.90/11.4
TPSSh	0.92/8.0	0.94/8.0	0.95/6.9	0.93/8.8
BMK	0.57	0.72	0.47	0.93/9.2
ωB97X-D	0.20	0.74	0.16	0.91/10.6
PBE0	0.74	0.92/9.5	0.72	0.94/7.5
M06-2X	0.29	0.55	0.27	0.90/10.3
PBE38	0.34	0.70	0.26	0.92/10.1
TPSS	0.91/10.2	0.94/8.2	0.91/10.2	0.90/10.6
PBE	0.90/11.0	0.94/8.6	0.90/10.6	0.88
B3LYP*	0.92/8.3	0.94/7.5	0.95/6.9	0.93/8.6
BP86	0.90/11.0	0.94/8.4	0.90/10.6	0.88
MN15	0.43	0.86	0.45	0.92/9.3
BHHLYP	0.20	0.56	0.14	0.71
B3LYP	0.79	0.85	0.88	0.91/9.2

Taking TPSSh as an example (Figure 4), the R^2 values of all four sets relative to the experimental data exceed 0.92, indicating a highly significant linear relationship. The second category contains the remaining functionals, for which only $E_{ad,u}$ shows a good linear correlation with the experimental values. In the case of BMK (Figure 5), for example, the R^2 of $E_{ad,u}$ reaches 0.93, whereas those of the other three are all below 0.75. It is worth noting that PBE0, although ostensibly belonging to the second category, has a significant outlier in its scatter plot (molecule **14**). Upon removal of this outlier, the R^2 values for both $E_{ad,u}$ and $E_{v,u}$ exceed 0.90, while those for the other two sets remain below 0.75. PBE0 therefore performs roughly in between the two

https://doi.org/10.1021/acs.jpca.4c08452
J. Phys. Chem. A 2025, 129, 2493−2509

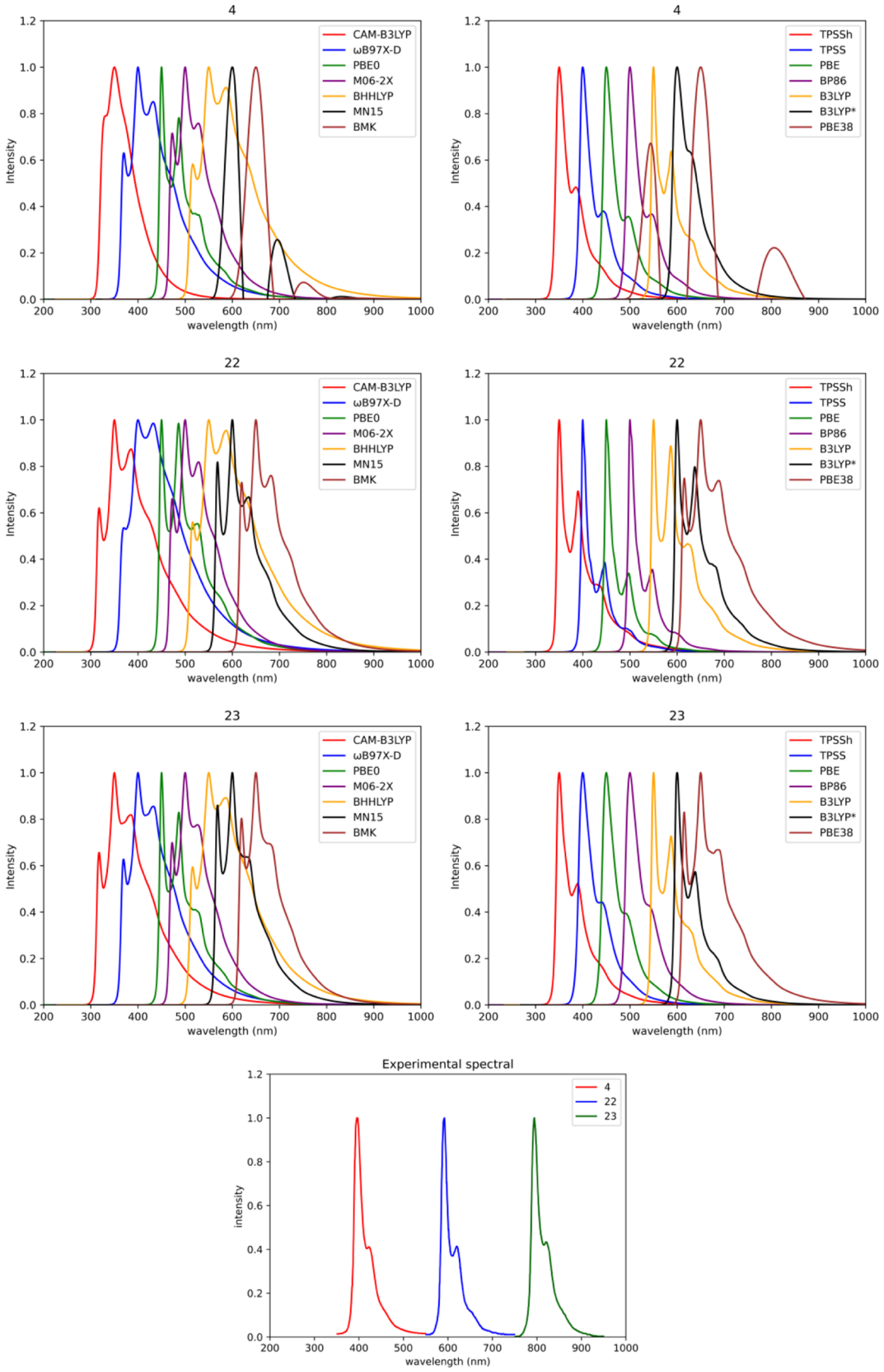

Figure 6. Calculated and experimental emission spectra of molecules **4**, **22** and **23**. All the spectra are shifted here for better visualization. Reproduced with permission.[38,70] Copyright 2014, Wiley-VCH. Copyright 2017, American Chemical Society.

categories mentioned above. All R^2 values are listed in Table 2, and for those larger than 0.90, corresponding MAR values are also provided. There are several sets that limit the error to less than 10 nm. Among them, TPSSh/$E_{ad,td}$ and B3LYP*/$E_{ad,td}$ perform the best. It is also worth noting that $E_{v,td}$, which results

https://doi.org/10.1021/acs.jpca.4c08452
J. Phys. Chem. A 2025, 129, 2493−2509

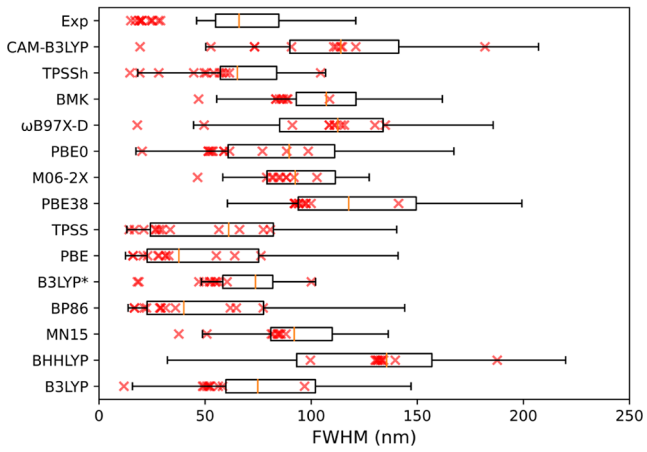

Figure 7. Calculated and experimental FWHM's of the emission spectra. Data of broadband molecules are shown as boxplots, while those of narrowband molecules are shown as red "x".

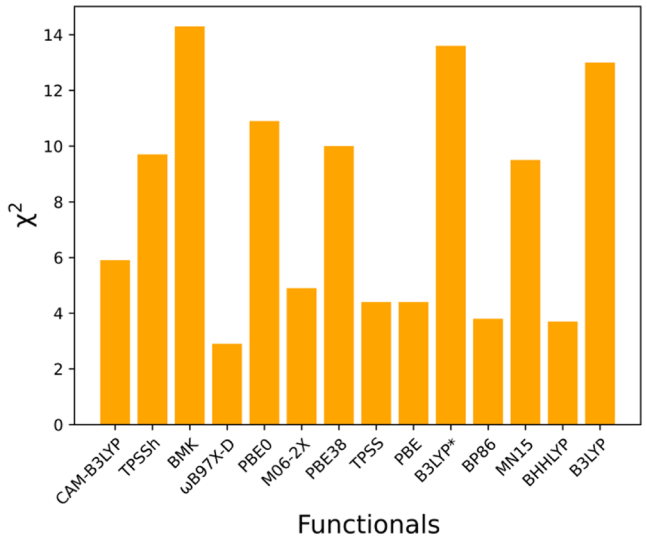

Figure 8. The χ^2 of each functional to distinguish between narrowband and broadband molecules.

from a single-point calculation of TDDFT and is commonly used, is not the best for any functional.

3.2. Emission Spectrum Shape. Based on the shape and width of the experimentally measured emission spectra, the 50 molecules studied in this work can be classified into two categories. The first category comprises molecules whose emission spectra feature a very narrow main peak, accompanied by a weak shoulder in the long-wavelength region. Due to the low intensity of the shoulder peak, these molecules exhibit FWHM of less than 30 nm and high color purity. A total of 12 molecules belong to this category: **4**, **10**, **11**, **17**, **18**, **19**, **22**, **23**, **31**, **45**, **46**, and **47**, and they will be referred to as narrowband molecules. The rest of the molecules belong to the second category, characterized by emission spectra that typically display a broad main peak and are usually without a distinct shoulder peak. These molecules all have FWHM's exceeding 45 nm and are called broadband molecules.

3.2.1. Comparison of Functionals. We calculate the vibrationally resolved emission spectra of the T_1 state for each functional and each molecule and compare their shapes with the experiment. We find that the spectral shapes predicted by

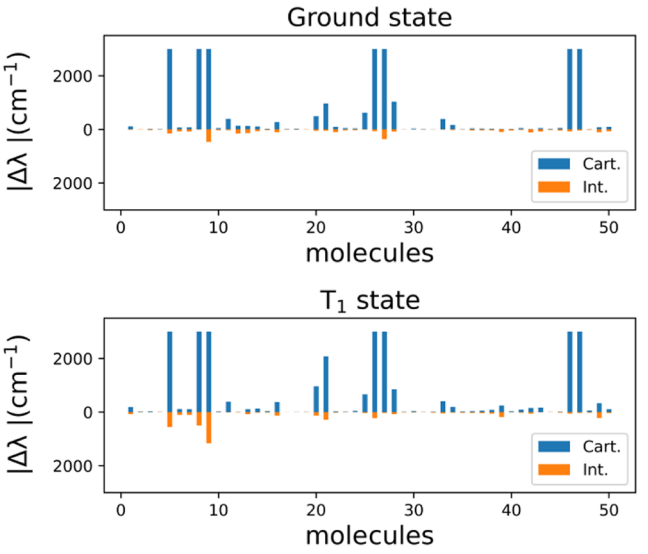

Figure 9. Difference between reorganization energies given by Cartesian coordinate, internal coordinate, and four-point method. Values over 3000 cm^{-1} are drawn as 3000 cm^{-1}.

TPSSh, TPSS, PBE, and BP86 are generally in better agreement with the experiment, especially for the narrowband molecules, followed by B3LYP* and B3LYP. As illustrative examples, the experimental and predicted spectra of molecules **4**, **22**, and **23** are presented in Figure 6. Since the emission wavelengths have been explored in the previous section, all spectra are appropriately shifted here for better visualization. It can be seen that the spectral shapes obtained using TPSSh, TPSS, PBE, and BP86 are in high agreement with the experimental spectra, differing only slightly in the relative intensities of the shoulder peaks. The spectra obtained using B3LYP and B3LYP* are of similar form but exhibit noticeably higher shoulder peaks, whereas the spectra given by the other functionals deviate significantly from the experiments. For molecule **4**, BMK, PBE38, and MN15 even give incorrect spectra that violate physical laws, indicating problematic results of electronic structure calculations. In fact, each functional gives unphysical spectra for a few molecules (e.g., with negative values, violently oscillating, or too broad), but there is a clear difference in the proportion of incorrect spectra produced by different functionals. The number of unphysical spectra given by TPSSh, TPSS, BP86, PBE, and B3LYP* does not exceed 5, showing good robustness for these molecules, while M06-2X and MN15 produce more than 10. A detailed list of molecules with problematic spectra can be found in Supporting Information.

To better demonstrate the relation between experimentally measured FWHM's and calculated ones for each functional, in Figure 7, the calculated FWHM's of broadband molecules are box-plotted, while those of narrowband molecules are plotted as red "x". The results show that the three pure functionals give FWHM's very close to the experiment for narrowband molecules, but tend to underestimate those for broadband molecules. In contrast, the boxplots of B3LYP, B3LYP*, and TPSSh align closely to the experimental data, indicating better performance for broadband molecules, but at the same time, they tend to predict the emission band of the narrowband molecules as wider. The remaining functionals yield FWHM's that are far from the experiment for both broadband and narrowband molecules. It seems that functionals with a small proportion of HF exchange give better predictions, which agrees

https://doi.org/10.1021/acs.jpca.4c08452
J. Phys. Chem. A 2025, 129, 2493−2509

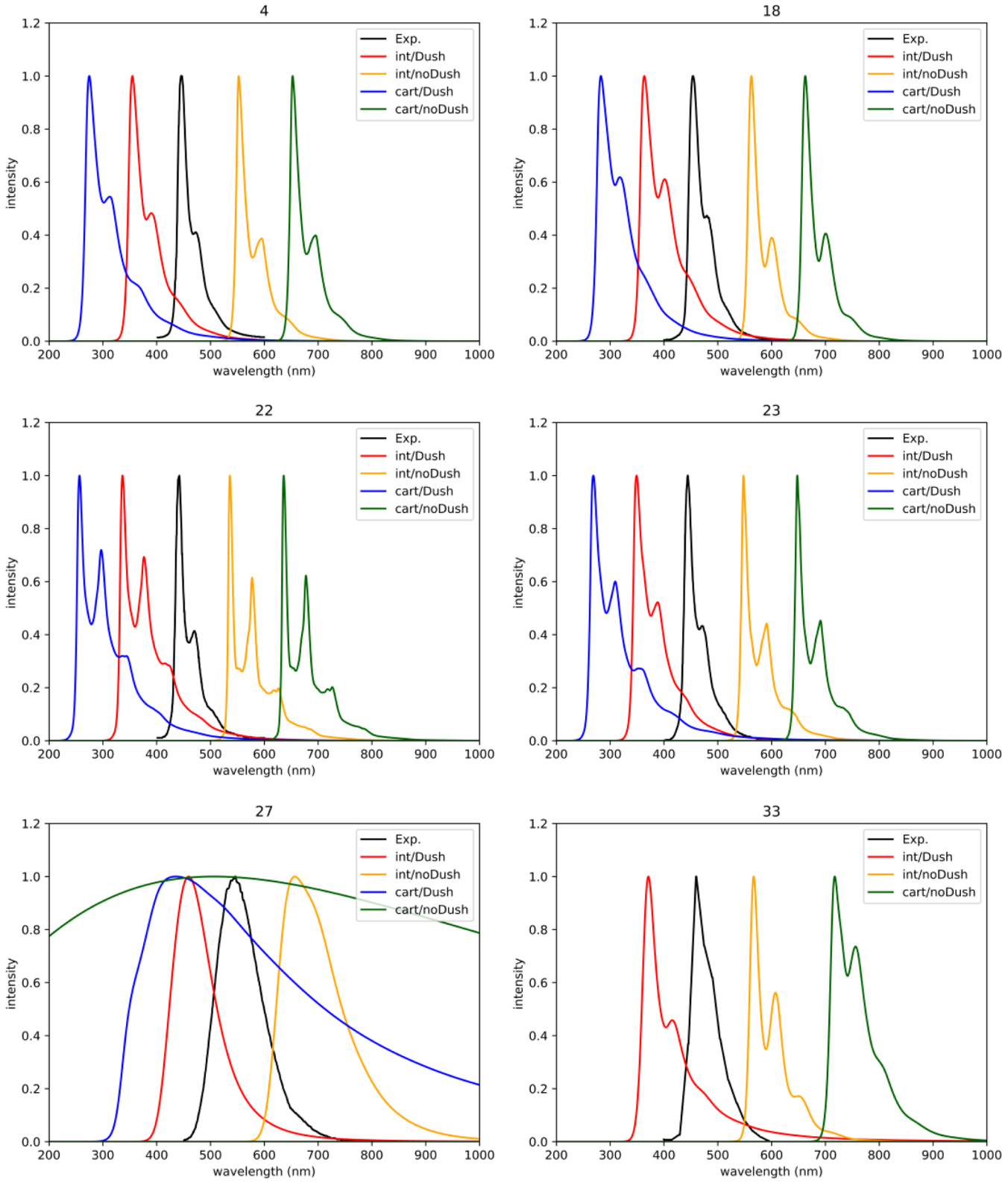

Figure 10. Calculated spectra of TPSSh functional with Cartesian/internal coordinate, with or without consideration of the Duschinsky rotation effect. All the spectra are shifted here for better visualization. Reproduced with permission. Copyright 2014, Wiley-VCH. Copyright 2022, Springer Nature. Copyright 2017, American Chemical Society. Copyright 2022, American Chemical Society.

with previous studies where B3PW91 with 20% HF exchange performs well for Pt(II) and Ir(III) complexes.[111,112]

However, the distributions of predicted FWHM of broadband and narrowband molecules always overlap, and no single functional can completely separate the two types of molecules. In order to quantitatively characterize the ability of each functional to distinguish between the two types of molecules, a χ^2 test is conducted. Specifically, a cutoff value A is chosen, and molecules with calculated FWHM larger than A are classified by this functional as broadband molecules, while those with

https://doi.org/10.1021/acs.jpca.4c08452
J. Phys. Chem. A 2025, 129, 2493−2509

Table 3. Molecules with Problematic Spectra Are Given by theFour Methods

molecules	DRE	DODF
Internal coordinates	9, 13, 20, 21, 28	None
Cartesian coordinates	8, 9, 26, 27, 33, 46, 47	9, 26, 27, 46, 47

FWHM smaller than A are classified as narrowband molecules. Further, depending on how well the prediction corresponds to the experiment, the χ^2 statistic of the functional can be calculated (see Supporting Information for details). A larger χ^2 indicates a greater ability of the functional to correctly distinguish between the two types of molecules. As shown in Figure 8, BMK, B3LYP*, and B3LYP provide the largest χ^2, followed by PBE0, PBE38, TPSSh, and MN15, consistent with the observations from Figure 7, where most of the red "x" in their plots falls to the left of the main box. The rest of the functionals perform poorly when distinguishing between the two types of molecules. Notably, for the three pure functionals, despite their good prediction of the spectral shapes of narrowband molecules, they still have small χ^2 due to poor performance for broadband molecules.

3.2.2. Cartesian Coordinate vs Internal Coordinate. To investigate the effect of the two coordinates, we employ the quantum chemical results of the TPSSh functional and calculate the reorganization energies using the two coordinates, respectively, which are defined by the difference between single-point energies of the same electronic state in two equilibrium structures. The reorganization energy can be estimated under harmonic approximation in both Cartesian and internal coordinates as

$$\lambda = \sum_i \frac{1}{2}\omega_i^2 \Delta Q_i^2 \tag{7}$$

where ω_i and ΔQ_i represent the vibrational frequency and mode displacement of normal mode i. It can also be directly calculated by quantum chemical software such as Gaussian, the latter also called the four-point method and is used as a reference here. All these results are listed in Table S3, and the residuals are plotted in Figure 9. It can be observed that the internal coordinate method gives reorganization energies in very good agreement with those of the four-point method, whereas the results of Cartesian coordinates are significantly less accurate. In particular, for several molecules containing flexible structures, such as molecules **5** and **9**, Cartesian coordinates give reorganization energies over 10,000 cm^{-1}, which is clearly incorrect and leads to excessively broad spectral predictions. Therefore, for molecules with flexible structures, only the internal coordinate method may provide reasonable spectra.

Further, we use the above TPSSh results to calculate emission spectra with both coordinates. For most molecules, especially for narrowband molecules, the spectral shapes obtained from the two coordinate systems show minimal differences. As shown in Figure 10, for **4**, **18**, and **23** molecules, the two methods give very similar spectral shapes , with only negligible differences in shoulder height, and they both agree well with experiments. For molecule **22**, they give a shoulder peak significantly higher than that of the experiment, but there is still little difference between themselves.

However, as mentioned above, for molecules with highly flexible structures, the results given by internal coordinates are significantly closer to the experimental values. Taking molecule **27** as an example, the spectrum obtained from Cartesian coordinates is excessively broad due to an unrealistically large reorganization energy. Internal coordinates, in contrast, produce results that align well with the experimental data. Besides, using Cartesian coordinates to calculate the spectra for molecule **33** results in a numeric error and program failure. In this case, internal coordinates give a spectrum in the same form as the experiment, although it is a little broader and with a lower shoulder.

3.2.3. DRE vs No DRE. To assess the importance of DRE in this system, we calculate the spectra under the DODF approximation using both coordinate methods and compare them with the results presented above. Under the DODF approximation, the Duschinsky rotation matrix is assumed to be identity, so that only the distribution of the reorganization energy among the vibrational modes affects the spectral shape. For most molecules, the inclusion of DRE does not significantly impact the form of the spectra. Specifically, as shown in Figure 8, taking DRE into account lowers the shoulder peaks of molecules **4**, **18**, **22**, and **23** to varying degrees, while it increases that of molecules **33**. Additionally, accounting for the DRE appears to slightly broaden the spectra of narrowband molecules, but this effect is minimal. However, this phenomenon is much more noticeable for molecule **27**, a broadband molecule, whether with Cartesian coordinates or internal coordinates. The calculated spectrum with Cartesian coordinates and DRE is much broader than that of the experiment, and the result of DODF is even worse.

However, DODF sometimes may rescue the calculation from failure. Calculations using Cartesian coordinates with DRE fail for molecule **33**, but DODF does give a spectrum close to the experiment, with only a slightly higher shoulder, suggesting that the Duschinsky rotation matrix derived from Cartesian coordinates may be problematic. This is noteworthy since molecule **33** is a narrowband molecule with reorganization energies smaller than 2000 cm^{-1}. It is well known that the internal coordinates method is more effective for flexible molecules because it typically gives smaller reorganization energies than the Cartesian coordinates method. But in this case, internal coordinates outperform Cartesian coordinates for a rigid molecule, not due to minor differences in reorganization energy, but because of the different Duschinsky rotation matrices they give.

In order to reveal the cause of the problematic spectra, the molecules with problematic spectra produced by the four methods are listed in Table 3. Even with DODF, Cartesian coordinates still give problematic spectra for five molecules, which suggests that the main problem may stem from the excessive reorganization energies. As Table S3 shows, all five molecules give reorganization energies over 5000 cm^{-1} when using Cartesian coordinates, which are far from the results of the four-point method. On the other hand, since the reorganization energies of all molecules using internal coordinates are below 3000 cm^{-1}, the failures of this method are likely due to problematic Duschinsky rotation matrices. Previous studies have reported that the Duschinsky rotation matrices given by the internal coordinates method are nonorthogonal,[63,102] which may contribute to the generation of problematic spectra. Another notable observation is that all the spectra containing negative values originate from the internal coordinates method, and these problems do disappear when applying DODF. Uncovering the cause of these problems remains challenging, but given that the inclusion of DRE has a minimal effect on the

https://doi.org/10.1021/acs.jpca.4c08452
J. Phys. Chem. A 2025, 129, 2493−2509

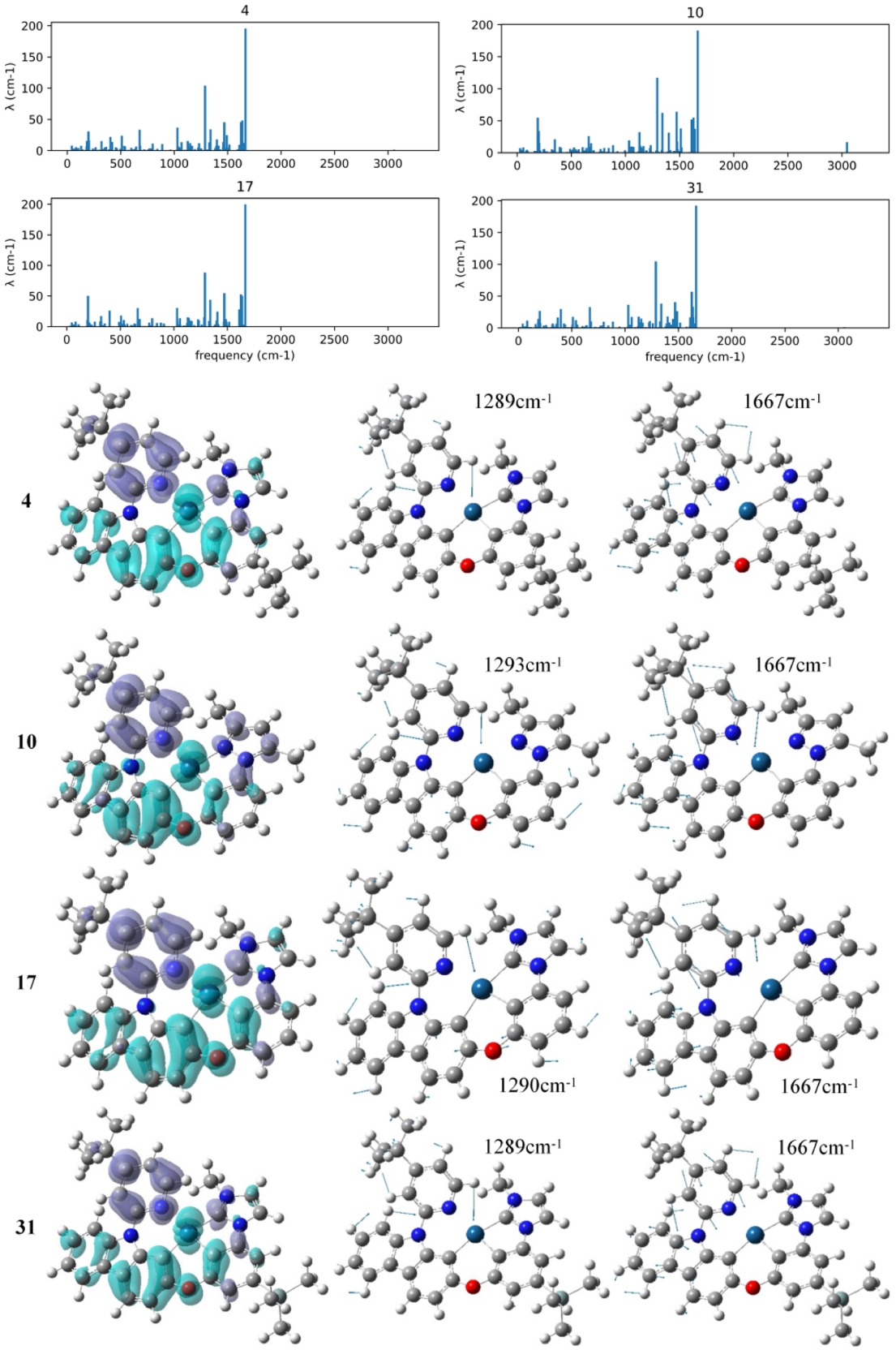

Figure 11. Bottom: CDD plots and the two modes with the largest reorganization energies for narrowband molecules **4**, **10**, **17**, and **31**. Purple/green shows where charge density increases/decreases in the S_0-T_1 transition (isovalue: 0.001). Top: reorganization energy distribution along vibrational modes.

spectral shape of most molecules, DODF may be a good method to improve the robustness of the calculations.

3.3. Electronic Structure and Vibrational Analysis. In order to elucidate the structure−property relationships of

https://doi.org/10.1021/acs.jpca.4c08452
J. Phys. Chem. A 2025, 129, 2493−2509

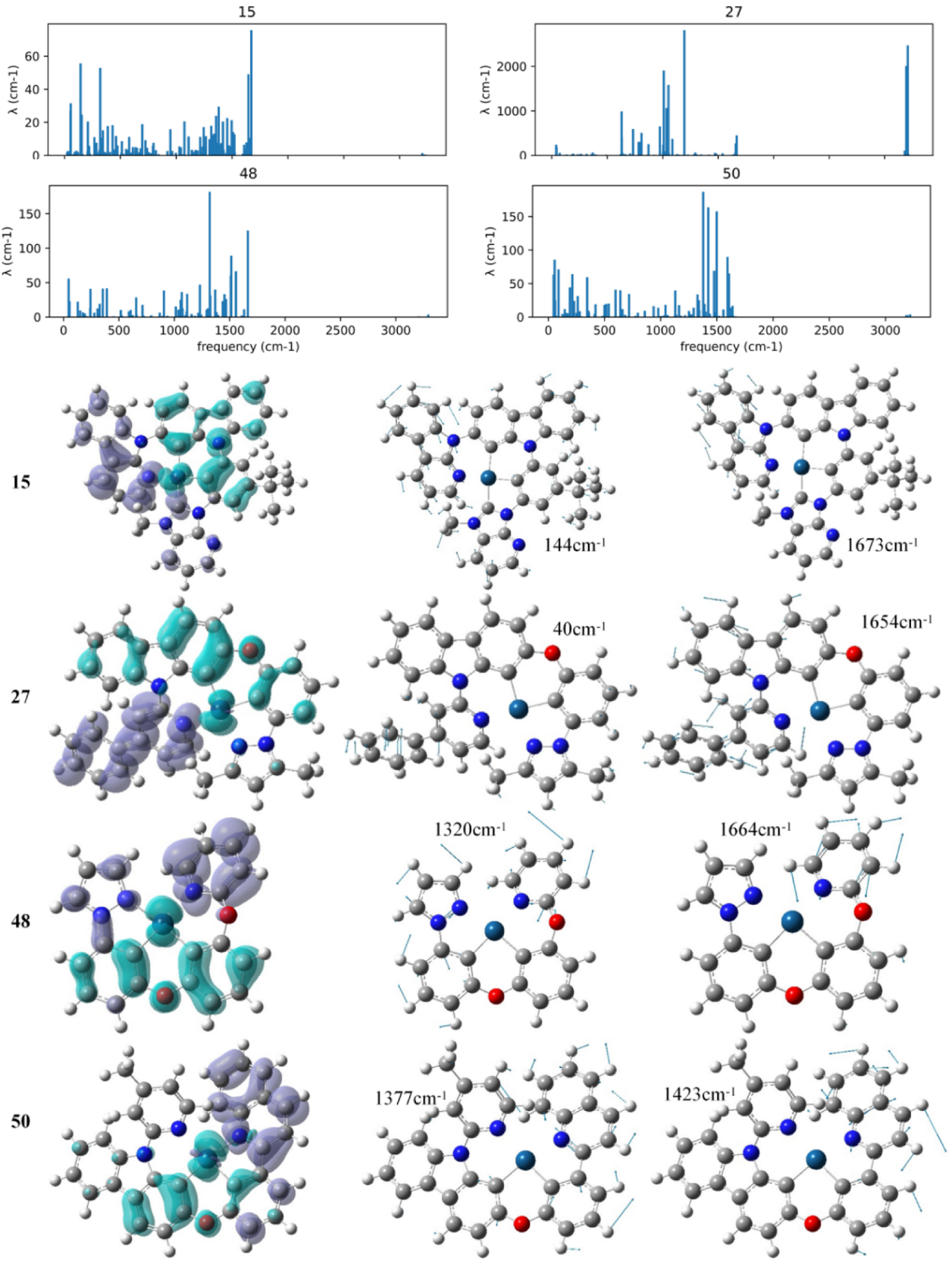

Figure 12. Bottom: CDD plots and the two modes with the largest reorganization energies for broadband molecules **15**, **27**, **48**, and **50**. Purple/green shows where charge density increases/decreases in S_0-T_1 transition (isovalue: 0.001). Top: reorganization energy distribution along vibrational modes.

tetradentate Pt(II) molecules and reveal the key factors affecting their color purity, we investigate the electronic structure and vibrational properties of several representative molecules in both the narrowband and broadband categories using the TPSSh functional.

https://doi.org/10.1021/acs.jpca.4c08452
J. Phys. Chem. A 2025, 129, 2493−2509

3.3.1. Narrowband Molecules. Here we select four representative molecules, **4**, **10**, **17**, and **31**, for our study. The emission spectra of all four molecules are narrow, and their shapes are correctly predicted by TPSSh. As shown in the CDD plots (Figure 11), the T_1 states of all four molecules display electron transfer from the platinum center and carbazole-oxygen moiety to pyridine. Meanwhile, their reorganization energies are predominantly concentrated in two vibrational modes near 1290 and 1667 cm^{-1}, which mainly correspond to the vibrations of the carbazole and pyridine groups. It is evident that the regions exhibiting electron density change are highly consistent with those associated with these vibrational modes. This correlation can be understood as follows: in regions where the electron density undergoes substantial alteration upon excitation, there is a corresponding significant change in the forces acting on the nuclei, leading to notable differences between the equilibrium structures of the two electronic states. Consequently, the reorganization energies are primarily distributed into the vibrational modes associated with these structural changes. In addition, these two vibrational modes should be the cause of the shoulder peak. The rest of the vibrational modes contribute minimal reorganization energies, and thus the main peak of the spectrum is very narrow.

3.3.2. Broadband Molecules. Here we choose molecules **15**, **27**, **48**, and **50** as examples for further study. As before, TPSSh correctly predicted their spectral shapes. As depicted in Figure 12, the nature of the electronic transitions of molecules **15**, **27**, and **50** differs markedly from that of the four narrowband molecules described previously. Although the electrons still transfer mainly from the platinum center and the carbazole moiety, the electron-accepting region is significantly larger due to the conjugation of the pyridine ring with other structures. Some low-frequency modes, which represent the overall deformation vibrations of the molecule, thus contribute significant reorganization energies. Activation of these low-frequency modes leads to a broadening of the main emission peak, which, together with the suppression of the vibrational mode around 1290 cm^{-1}, results in a spectrum that no longer exhibits significant shoulder peaks. In addition, there are several molecules that display spectral shapes with very high shoulder peaks, such as **48**, where electron transfer occurs mainly from the two benzene rings due to the absence of the carbazole unit. The vibrational modes associated with these benzene rings are significantly different from those of carbazole, resulting in a high shoulder peak in the emission spectrum.

Based on the analysis above, it can be concluded that the presence of the pyridine-carbazole-oxygen moiety is a key factor in achieving high color purity in these tetradentate Pt(II) molecules, where the pyridine group should not conjugate with other structures. Since the electron density changes mainly in this unit, only two specific high-frequency vibrational modes are activated, producing low shoulder peaks in the spectra, whereas the low-frequency modes contribute little reorganization energy, allowing the main peaks to be narrow. Otherwise, when other structures participate significantly in electron transfer, the low-frequency vibrational modes are likely to be activated, leading to a broadening of the spectrum and a decrease in color purity. From the experimental results, all 12 narrowband molecules in our data set possess the pyridine-carbazole-oxygen moiety. Moreover, recent syntheses of 11 tetradentate Pt(II) complexes not included in our data set further corroborate this trend. Among these new molecules, the three containing the pyridine-carbazole-oxygen moiety exhibit very high color purity,[103,104] while the other eight molecules lacking this structure exhibit low color purity.[105,106] Therefore, we assert that the pyridine-carbazole-oxygen moiety is essential for achieving high color purity in these tetradentate Pt(II) molecules.

4. CONCLUSION

Using DFT, UDFT, and TDDFT methods, we investigated the performance of 14 different functionals for calculating the photophysical properties of 50 tetradentate Pt(II) molecules in dichloromethane solution. The adiabatic energy gap calculated using (U)B3LYP* exhibits the smallest error (-0.02 ± 0.06 eV) relative to the experimentally measured phosphorescence emission peak energies. Besides, the adiabatic energy gap calculated using either the TD-TPSSh or TD-B3LYP* method shows the best conformity with the experimental trend, yielding an average absolute residual of 6.9 nm after linear fitting. By combining these methods with FGR and TVCF, we find that the computed spectral shapes using the TPSSh, TPSS, BP86, and PBE functionals are in good agreement with the experiments. Overall, the use of the internal coordinate method effectively improves the spectral calculations by providing more accurate reorganization energies compared to Cartesian coordinates, although at the cost of slightly reduced robustness in the Duschinsky rotation matrices. The differences between the spectra obtained with the linear Duschinsky relation and those with the DODF model are generally insignificant, indicating that the spectral shape is not affected much by DRE for most molecules.

Furthermore, by analyzing the electronic structures and vibrational properties, we have identified the pyridine-carbazole-oxygen moiety as a crucial structural unit for achieving high color purity in such molecules. When the T_1 state mainly exhibits electron transfer from the platinum and carbazole-oxygen structure to pyridine, two vibrational modes near 1290 and 1667 cm^{-1} are activated and produce a low shoulder peak in the emission spectrum. Meanwhile, the low-frequency vibrational modes are suppressed, keeping the main peak narrow. In contrast, when electron transfer in the T_1 state involves other structures, more low-frequency modes are activated, resulting in a broadening of the main peak and a decrease in color purity. This work will help with understanding the structure−property relationship of Pt complexes and will contribute to more efficient screening and synthesis of molecules and OLED devices with high color purity.

■ ASSOCIATED CONTENT

Supporting Information

The Supporting Information is available free of charge at https://pubs.acs.org/doi/10.1021/acs.jpca.4c08452.

The dispersion correction parameters of each functional and experimental values. The data lists and scatter plots of emission energies and FWHM of spectra calculated with each functional. (docx) (PDF)

The spectra calculated with each functional or with each potential energy surface model. (docx) (PDF)

Spectra of TPSSh with different potential energy surface models. Dush represents AH model with full consideration of linear Duschinsky relation, while noDu represents DODF model. Int and cart represent internal coordinates and Cartesian coordinates respectively (PDF)

https://doi.org/10.1021/acs.jpca.4c08452
J. Phys. Chem. A 2025, 129, 2493−2509

AUTHOR INFORMATION

Corresponding Author

Zhigang Shuai − *Department of Chemistry, MOE Key Laboratory of Organic OptoElectronics and Molecular Engineering, Tsinghua University, Beijing 100084, China; School of Science and Engineering, The Chinese University of Hong Kong, Shenzhen, Guangdong 518172, China;* orcid.org/0000-0003-3867-2331; Email: shuaizhigang@cuhk.edu.cn

Authors

Xiao Chen − *Department of Chemistry, MOE Key Laboratory of Organic OptoElectronics and Molecular Engineering, Tsinghua University, Beijing 100084, China;* orcid.org/0009-0004-4824-5928

Shanhao Deng − *Department of Chemistry, MOE Key Laboratory of Organic OptoElectronics and Molecular Engineering, Tsinghua University, Beijing 100084, China*

Wenjie Zhang − *Department of Chemistry, MOE Key Laboratory of Organic OptoElectronics and Molecular Engineering, Tsinghua University, Beijing 100084, China*

Pingan Yin − *Department of Chemistry, MOE Key Laboratory of Organic OptoElectronics and Molecular Engineering, Tsinghua University, Beijing 100084, China*

Weitang Li − *School of Science and Engineering, The Chinese University of Hong Kong, Shenzhen, Guangdong 518172, China*

Complete contact information is available at: https://pubs.acs.org/10.1021/acs.jpca.4c08452

Author Contributions

The manuscript was written with contributions from all authors. All authors have given approval to the final version of the manuscript.

Notes

The authors declare no competing financial interest.

ACKNOWLEDGMENTS

This work is supported by the National Natural Science Foundation of China (grant nos. T2350009 and 22433007), the Guangdong Provincial Natural Science Foundation (grant nos. 2024A1515011185), and the Shenzhen City Peacock Team Project (grant no. KQTD20240729102028011). W.L. is supported by the University Development Fund (no. DF01003789) and the Young Elite Scientists Sponsorship Program by the China Association of Science and Technology (no. 2023QNRC001).

REFERENCES

(1) Hong, G.; Gan, X. M.; Leonhardt, C.; Zhang, Z.; Seibert, J.; Busch, J. M.; Bräse, S. A Brief History of OLEDs—Emitter Development and Industry Milestones. *Adv. Mater.* **2021**, *33* (9), 2005630.

(2) Zhu, Z. Q.; Klimes, K.; Holloway, S.; Li, J. Efficient Cyclometalated Platinum(II) Complex with Superior Operational Stability. *Adv. Mater.* **2017**, *29* (6), 1605002.

(3) Lai, S. L.; Tong, W. Y.; Kui, S. C. F.; Chan, M. Y.; Kwok, C. C.; Che, C. M. High Efficiency White Organic Light-Emitting Devices Incorporating Yellow Phosphorescent Platinum(II) Complex and Composite Blue Host. *Adv. Funct. Mater.* **2013**, *23* (41), 5168−5176.

(4) Li, B. N.; Li, Y. G.; Chan, M. H. Y.; Yam, V. W. W. Phosphorescent Cyclometalated Platinum(II) Enantiomers with Circularly Polarized Luminescence Properties and Their Assembly Behaviors. *J. Am. Chem. Soc.* **2021**, *143* (51), 21676−21684.

(5) Dragonetti, C.; Fagnani, F.; Marinotto, D.; di Biase, A.; Roberto, D.; Cocchi, M.; Fantacci, S.; Colombo, A. First member of an appealing class of cyclometalated 1,3-di-(2-pyridyl)benzene platinum(ii) complexes for solution-processable OLEDs. *J. Mater. Chem. C* **2020**, *8* (23), 7873−7881.

(6) Chan, A. K. W.; Lam, E. S. -H.; Tam, A. Y. -Y.; Tsang, D. P. K.; Lam, W. H.; Chan, M. Y.; Wong, W. T.; Yam, V. W. -W. Synthesis and Characterization of Luminescent Cyclometalated Platinum(II) Complexes of 1,3-Bis-Hetero-Azolylbenzenes with Tunable Color for Applications in Organic Light-Emitting Devices through Extension of π Conjugation by Variation of the Heteroatom. *Chem. - Eur. J.* **2013**, *19* (41), 13910−13924.

(7) Wang, L.; Miao, J. S.; Zhang, Y. M.; Wu, C. J.; Huang, H.; Wang, X. Z.; Yang, C. L. Discrete Mononuclear Platinum(II) Complexes Realize High-Performance Red Phosphorescent OLEDs with EQEs of up to 31.8% and Superb Device Stability. *Adv. Mater.* **2023**, *35* (32), 9.

(8) Zhang, H.; Liu, C.; Du, C.; Zhang, B. Efficiently red emitting cycloplatinated(II) complexes supported by N∧O and N∧P benzimidazole ancillary ligands. *J. Organomet. Chem.* **2022**, *960*, 122237.

(9) Yuen, M. -Y.; Kui, S. C. E.; Low, K. -H.; Kwok, C. C.; Chui, S. S. Y.; Ma, C. -W.; Zhu, N. Y.; Che, C. -M. Synthesis, Photophysical and Electrophosphorescent Properties of Fluorene-Based Platinum(II) Complexes. *Chem.-Eur. J.* **2010**, *16* (47), 14131−14141.

(10) Mao, M.; Peng, J. H.; Lam, T. L.; Ang, W. H.; Li, H. Y.; Cheng, G.; Che, C. M. High-performance organic light-emitting diodes with low-efficiency roll-off using bulky tetradentate Pt(ONCN) emitters. *J. Mater. Chem. C* **2019**, *7* (24), 7230−7236.

(11) Tao, W. T.; Chen, Y.; Lu, L.; Liu, C. Luminescence properties of cyclometalated platinum(II) complexes in a dichloromethane/n-hexane system. *Tetrahedron Lett.* **2021**, *66*, 152802.

(12) Zhang, J.; Dai, G. L.; Wu, F. S.; Li, D.; Gao, D. C.; Jin, H. W.; Chen, S.; Zhu, X. J.; Huang, C. X.; Han, D. M. Efficient and tunable phosphorescence of new platinum(II) complexes based on the donor-π-acceptor Schiff bases. *J. Photochem. Photobiol., A* **2016**, *316*, 12−18.

(13) Luo, Z. L.; Liu, Y. G.; Tong, K. C.; Chang, X. Y.; To, W. P.; Che, C. M. Luminescent Platinum(II) Complexes with Bidentate Diacetylide Ligands: Structures, Photophysical Properties and Application Studies. *Chem.-Asian J.* **2021**, *16* (19), 2978−2992.

(14) Kourkoulos, D.; Karakus, C.; Hertel, D.; Alle, R.; Schmeding, S.; Hummel, J.; Risch, N.; Holder, E.; Meerholz, K. Photophysical properties and OLED performance of light-emitting platinum(II) complexes. *Dalton Trans.* **2013**, *42* (37), 13612−13621.

(15) Yang, X. L.; Xu, X. B.; Zhao, J.; Dang, J. S.; Huang, Z.; Yan, X. G.; Zhou, G. J.; Wang, D. D. Phosphorescent Platinum(II) Complexes Bearing 2-Vinylpyridine-type Ligands: Synthesis, Electrochemical and Photophysical Properties, and Tuning of Electrophosphorescent Behavior by Main-Group Moieties. *Inorg. Chem.* **2014**, *53* (24), 12986−13000.

(16) Hu, Z. Y.; Wang, Y. F.; Shi, D. Y.; Tan, H.; Li, X. S.; Wang, L.; Zhu, W. G.; Cao, Y. Highly-efficiency red-emitting platinum (II) complexes containing 4′-diarylamino-1-phenylisoquinoline ligands in polymer light-emitting diodes: Synthesis, structure, photoelectron and electroluminescence. *Dyes Pigment* **2010**, *86* (2), 166−173.

(17) Zhang, H. -H.; Yang, Q. -Y.; Qi, X. -W.; Sun, S. -S.; Li, B. -S.; Zhang, D. -S.; Zhang, X. -P.; Shi, Z. -F. Improved mechanochromism and mechanoluminescence in fluoro-substituted N″N″C-coordinating cyclometalated platinum (II) complexes. *Inorg. Chim. Acta* **2021**, *523*, 120411.

(18) Wen, H. M.; Wang, J. Y.; Li, B.; Zhang, L. Y.; Chen, C. N.; Chen, Z. N. Phosphorescent Square-Planar Platinum(II) Complexes of 1,3-Bis(2-pyridylimino)isoindoline with a Monodentate Strong-Field Ligand. *Eur. J. Inorg. Chem.* **2013**, *2013* (27), 4789−4798.

(19) Fecková, M.; Kahlal, S.; Roisnel, T.; Saillard, J. Y.; Boixel, J.; Hruzd, M.; le Poul, P.; Gauthier, S.; Robin-le Guen, F.; Bures, F. Cyclometallated 2-Phenylpyrimidine Derived Platinum Complexes: Synthesis and Photophysical Properties. *Eur. J. Inorg. Chem.* **2021**, *2021* (16), 1592−1600.

(20) Soellner, J.; Strassner, T. Phosphorescent Cyclometalated Platinum(II) aNHC Complexes. *Chem.-Eur. J.* **2018**, *24* (58), 15603−15612.
(21) Shigehiro, T.; Chen, Q.; Yagi, S.; Maeda, T.; Nakazumi, H.; Sakurai, Y. Substituent effect on photo- and electroluminescence properties of heteroleptic cyclometalated platinum(II) complexes based on a 2-(dibenzo[b,d]furan-4-yl)pyridine ligand. *Dyes Pigment* **2016**, *124*, 165−173.
(22) Begantsova, Y. E.; Bochkarev, L. N.; Ketkov, S. Y.; Baranov, E. V.; Bochkarev, M. N.; Yakhvarov, D. G. Synthesis, characterization and photophysical properties of new cyclometallated platinum(II) complexes with pyrazolonate ancillary ligand. *J. Organomet. Chem.* **2013**, *733*, 1−8.
(23) Lanoë, P. H.; Moreno-Betancourt, A.; Wilson, L.; Philouze, C.; Monnereau, C.; Jamet, H.; Jouvenot, D.; Loiseau, F. Neutral heteroleptic cyclometallated Platinum(II) complexes featuring 2-phenylbenzimidazole ligand as bright emitters in solid state and in solution. *Dyes Pigment* **2019**, *162*, 967−977.
(24) Zhang, Y. M.; Chen, Z.; Wang, X.; He, J. J.; Wu, J. T.; Liu, H. Y.; Song, J.; Qu, J. L.; Chan, W. T. K.; Wong, W. Y. Achieving NIR Emission for Donor-Acceptor Type Platinum(II) Complexes by Adjusting Coordination Position with Isomeric Ligands. *Inorg. Chem.* **2018**, *57* (22), 14208−14217.
(25) Naziruddin, A. R.; Galstyan, A.; Iordache, A.; Daniliuc, C. G.; Strassert, C. A.; De Cola, L. Bidentate NHC pyrozolate ligands in luminescent platinum(II) complexes. *Dalton Trans.* **2015**, *44* (18), 8467−8477.
(26) Soellner, J.; Strassner, T. Mesoionic 1,2,3-Triazolo[1,5-a]-pyridine-3-ylidenes in Phosphorescent Platinum(II) Complexes. *ChemPhotochem* **2019**, *3* (10), 1000−1003.
(27) Shi, L. L.; Li, T.; Zhao, S. S.; Li, H.; Su, Z. M. The effect of phenyl group on the electronic and phosphorescent properties of cyclometalated analogues of platinum(II) terpyridine complexes: A theoretical study. *Theor. Chem. Acc.* **2009**, *124* (1−2), 29−36.
(28) Wang, Y. X.; Guo, Z. L.; Gao, Y. X.; Tian, Y. R.; Deng, Y. Y.; Ma, X. A.; Yang, W. S. Tuning Hybridized Local and Charge-Transfer Mixing for Efficient Hot-Exciton Emission with Improved Color Purity. *J. Phys. Chem. Lett.* **2022**, *13* (29), 6664−6673.
(29) Xiong, X.; Cheng, Y. C.; Wang, K.; Yu, J.; Zhang, X. H. A comparative study of two multi-resonance TADF analogous materials integrating chalcogen atoms of different periods. *Mater. Chem. Front.* **2023**, *7* (5), 929−936.
(30) Kataoka, Y.; Kitagawa, Y.; Kawakami, T.; Okumura, M. Photophysical properties of mono- and di-nuclear platinum(II) complexes with the tridentate ligand 2-phenyl-6-(1H-pyrazol-3-yl)-pyridine: A DFT and TDDFT study. *J. Organomet. Chem.* **2013**, *743*, 163−169.
(31) Han, D. M.; Li, J. M.; Pang, C. Y.; Zhao, L. H.; Xia, B.; Zhang, G. Theoretical Investigation on the Electronic Structures and Optoelectronic Properties of a Series of Platinum(II) Complexes with Different Substituent Groups. *Mol. Cryst. Liq. Cryst.* **2015**, *616* (1), 133−142.
(32) Han, D. M.; Wu, Y. H.; Cai, H. X.; Pang, C. Y.; Zhao, L. H. DFT/TDDFT investigation on the electronic structures and photophysical properties of a series of substituted N-heterocyclic carbene (NHC) platinum(II) complexes. *Synth. Met.* **2015**, *209*, 455−460.
(33) Shang, X. H.; Han, D. M.; Wan, N.; Zhou, D. F.; Zhang, G. DFT/TDDFT investigation on the electronic structures and photophysical properties of phosphorescent platinum(II) complexes with triarylboron/triarylnitrogen-functionalized N-heterocyclic carbene chelate ligands. *Chem. Phys. Lett.* **2015**, *635*, 217−223.
(34) Han, D. M.; He, X. X.; Zhao, L. H.; Pang, C. Y.; Yu, Y. H.; Zhang, G. Theoretical investigation on the electronic structures and phosphorescent properties of a series of cyclometalated platinum(II) complexes with different substituted N-heterocyclic carbene ligands. *Mol. Cryst. Liq. Cryst.* **2016**, *625* (1), 202−211.
(35) Du, J. H.; Luo, Y. F.; Xie, X. H.; Hu, W. H.; Shen, W. Tuning the electronic and photophysical properties of platinum(II) complexes through ancillary ligand modification: A theoretical study. *Mol. Simul.* **2016**, *42* (12), 1035−1041.
(36) Yan, X.; Li, W.; Zhang, H.; Cai, W.; Wang, J.; Shen, W. DFT/TDDFT insight into the impact of ring size of the NHC chelating unit of high effective phosphorescent Platinum (II) complexes. *Appl. Organomet. Chem.* **2018**, *32* (9), No. e4467.
(37) Luo, Y. F.; Guo, Y.; Shou, X. C.; Chen, Z. Z.; Xu, Z. G.; Tang, D. Y. Investigate the Relationship between Structure and Triplet Potential Energy Surface to Control the Phosphorescence Quantum Yield of Platinum(II) Complex: A Theoretical Investigation. *Inorg. Chem* **2022**, *61* (24), 9162−9172.
(38) Fleetham, T.; Li, G.; Wen, L.; Li, J. Efficient "Pure" Blue OLEDs Employing Tetradentate Pt Complexes with a Narrow Spectral Bandwidth. *Adv. Mater.* **2014**, *26* (41), 7116−7121.
(39) Kim, J. M.; Cheong, K.; Jiang, J. X.; Jeon, S. O.; Hong, W. P.; Lee, J. Y. Tetradentate Pt complexes for organic light-emitting diodes. *Trends Chem.* **2023**, *5* (4), 267−278.
(40) Sun, J.; Ahn, H.; Kang, S.; Ko, S. B.; Song, D.; Um, H. A.; Kim, S.; Lee, Y.; Jeon, P.; Hwang, S. H. Exceptionally stable blue phosphorescent organic light-emitting diodes. *Nat. Photonics* **2022**, *16* (3), 212−218.
(41) Strickler, S. J.; Berg, R. A. RELATIONSHIP BETWEEN ABSORPTION INTENSITY AND FLUORESCENCE LIFETIME OF MOLECULES. *J. Chem. Phys.* **1962**, *37* (4), 814−822.
(42) Sharp, T. E.; Rosenstock, H. M. FRANCK-CONDON FACTORS FOR POLYATOMIC MOLECULES. *J. Chem. Phys.* **1964**, *41* (11), 3453−3463.
(43) Ou, Q.; Peng, Q.; Shuai, Z. Computational screen-out strategy for electrically pumped organic laser materials. *Nat. Commun.* **2020**, *11* (1), 4485.
(44) Lin, S. Y.; Ou, Q.; Peng, Q.; Shuai, Z. G. Computational studies on the excited state decay rates in aggregates of two-coordinate Cu (I) complexes: Thermally Activated Delayed Fluorescence and Aggregation Induced Emis. *J. Chin. Chem. Soc.* **2023**, *70* (3), 287−296.
(45) Shuai, Z. G.; Peng, Q. Excited states structure and processes: Understanding organic light-emitting diodes at the molecular level. *Phys. Rep.-Rev. Sec. Phys. Lett.* **2014**, *537* (4), 123−156.
(46) Sun, Q.; Ren, J.; Peng, Q.; Shuai, Z. Heterofission Mechanism for Pure Organic Room Temperature Phosphorescence. *Adv. Opt. Mater.* **2024**, *12* (5), 2301769.
(47) Niu, Y. L.; Li, W. Q.; Peng, Q.; Geng, H.; Yi, Y. P.; Wang, L. J.; Nan, G. J.; Wang, D.; Shuai, Z. G. MOlecular MAterials Property Prediction Package (MOMAP) 1.0: A software package for predicting the luminescent properties and mobility of organic functional materials. *Mol. Phys.* **2018**, *116* (7−8), 1078−1090.
(48) Niu, Y.; Peng, Q.; Shuai, Z. Promoting-mode free formalism for excited state radiationless decay process with Duschinsky rotation effect. *Sci. China, Ser. B:Chem.* **2008**, *51* (12), 1153−1158.
(49) Shuai, Z. G. Thermal Vibration Correlation Function Formalism for Molecular Excited State Decay Rates. *Chin. J. Chem.* **2020**, *38* (11), 1223−1232.
(50) Peng, Q.; Yi, Y. P.; Shuai, Z. G.; Shao, J. S. Toward quantitative prediction of molecular fluorescence quantum efficiency: Role of Duschinsky rotation. *J. Am. Chem. Soc.* **2007**, *129* (30), 9333−9339.
(51) Wang, Y.; Peng, Q.; Shuai, Z. G. A computational scheme for evaluating the phosphorescence quantum efficiency: Applied to blue-emitting tetradentate Pt(ii) complexes. *Mater. Horiz.* **2022**, *9* (1), 334−341.
(52) Hagai, M.; Inai, N.; Yasuda, T.; Fujimoto, K. J.; Yanai, T. Extended theoretical modeling of reverse intersystem crossing for thermally activated delayed fluorescence materials. *Sci. Adv.* **2024**, *10* (5), 10.
(53) Cerezo, J.; Santoro, F. FCclasses3: Vibrationally-resolved spectra simulated at the edge of the harmonic approximation. *J. Comput. Chem.* **2023**, *44* (4), 626−643.
(54) de Souza, B.; Neese, F.; Izsák, R. On the theoretical prediction of fluorescence rates from first principles using the path integral approach. *J. Chem. Phys.* **2018**, *148* (3), 034104.
(55) Muniz-Miranda, F.; Pedone, A.; Battistelli, G.; Montalti, M.; Bloino, J.; Barone, V. Benchmarking TD-DFT against Vibrationally Resolved Absorption Spectra at Room Temperature: 7-Amino-

https://doi.org/10.1021/acs.jpca.4c08452
J. Phys. Chem. A 2025, 129, 2493−2509

coumarins as Test Cases. *J. Chem. Theory Comput.* **2015**, *11* (11), 5371−5384.
(56) Laurent, A. D.; Jacquemin, D. TD-DFT benchmarks: A review. *Int. J. Quantum Chem.* **2013**, *113* (17), 2019−2039.
(57) Jacquemin, D.; Wathelet, V.; Perpète, E. A.; Adamo, C. Extensive TD-DFT Benchmark: Singlet-Excited States of Organic Molecules. *J. Chem. Theory Comput.* **2009**, *5* (9), 2420−2435.
(58) Jacquemin, D.; Perpete, E. A.; Scuseria, G. E.; Ciofini, I.; Adamo, C. TD-DFT performance for the visible absorption spectra of organic dyes: Conventional versus long-range hybrids. *J. Chem. Theory Comput.* **2008**, *4* (1), 123−135.
(59) Jacquemin, D.; Perpete, E. A.; Vydrov, O. A.; Scuseria, G. E.; Adamo, C. Assessment of long-range corrected functionals performance for n→π^* transitions in organic dyes. *J. Chem. Phys.* **2007**, *127* (9), 094102.
(60) Reimers, J. R. A practical method for the use of curvilinear coordinates in calculations of normal-mode-projected displacements and Duschinsky rotation matrices for large molecules. *J. Chem. Phys.* **2001**, *115* (20), 9103−9109.
(61) Borrelli, R.; Peluso, A.; Peluso, A. The vibrational progressions of the N→V electronic transition of ethylene: A test case for the computation of Franck-Condon factors of highly flexible photoexcited molecules. *J. Chem. Phys.* **2006**, *125* (19), 194308.
(62) Capobianco, A.; Borrelli, R.; Noce, C.; Peluso, A.; Peluso, A. Franck−Condon factors in curvilinear coordinates: The photoelectron spectrum of ammonia. *Theor. Chem. Acc.* **2012**, *131* (3), 1181.
(63) Cerezo, J.; Zúñiga, J.; Requena, A.; Ferrer, F. J. A.; Santoro, F. Harmonic Models in Cartesian and Internal Coordinates to Simulate the Absorption Spectra of Carotenoids at Finite Temperatures. *J. Chem. Theory Comput.* **2013**, *9* (11), 4947−4958.
(64) Hang, X. C.; Fleetham, T.; Turner, E.; Brooks, J.; Li, J. Highly Efficient Blue-Emitting Cyclometalated Platinum(II) Complexes by Judicious Molecular Design. *Angew. Chem., Int. Ed.* **2013**, *52* (26), 6753−6756.
(65) Li, J.; Liang, F.; Zhao, Y.; Liu, X. Y.; Fan, J.; Liao, L. S. Highly phosphorescent cyclometalated platinum(II) complexes based on 2-phenylbenzimidazole-containing ligands. *J. Mater. Chem. C* **2017**, *5* (25), 6202−6209.
(66) Yu, F. L.; Sheng, Y. J.; Wu, D. D.; Qin, K.; Li, H. B.; Xie, G. H.; Xue, Q.; Sun, Z. Y.; Lu, Z. Z.; Ma, H. L. Blue-Phosphorescent Pt(II) Complexes of Tetradentate Pyridyl-Carbolinyl Ligands: Synthesis, Structure, Photophysics, and Electroluminescence. *Inorg. Chem.* **2020**, *59* (19), 14493−14500.
(67) Li, G.; Ameri, L.; Fleetham, T.; Zhu, Z. -Q.; Li, J. Stable and efficient blue and green organic light emitting diodes employing tetradentate Pt(II) complexes. *Appl. Phys. Lett.* **2020**, *117* (25), 253301.
(68) Li, G. J.; Liu, S.; Sun, Y. L.; Lou, W. W.; Yang, Y. F.; She, Y. B. N-Heterocyclic carbene-based tetradentate platinum(ii) complexes for phosphorescent OLEDs with high brightness. *J. Mater. Chem. C* **2021**, *10* (1), 210−218.
(69) Li, G. J.; Klimes, K.; Fleetham, T.; Zhu, Z. Q.; Li, J. Stable and efficient sky-blue organic light emitting diodes employing a tetradentate platinum complex. *Appl. Phys. Lett.* **2017**, *110* (11), 5.
(70) Li, G. J.; Wolfe, A.; Brooks, J.; Zhu, Z. Q.; Li, J. Modifying Emission Spectral Bandwidth of Phosphorescent Platinum(II) Complexes Through Synthetic Control. *Inorg. Chem.* **2017**, *56* (14), 8244−8256.
(71) Zhu, L.; Xie, W. T.; Qian, C. Y.; Xie, W.; Shen, K.; Lv, A. Q.; Ma, H. L.; Li, H. B.; Hang, X. C.; Li, W. Q.; et al. Tetradentate Pt(II) Complexes for Spectrum-Stable Deep-Blue and White Electroluminescence. *Adv. Opt. Mater.* **2020**, *8* (19), 2000406.
(72) Park, H. J.; Jang, J. H.; Lee, J. H.; Hwang, D. Highly Efficient Deep-Blue Phosphorescent OLEDs Based on a Trimethylsilyl-Substituted Tetradentate Pt(II) Complex. *ACS Appl. Mater. Interfaces* **2022**, *14* (30), 34901−34908.
(73) Zhu, L.; Sha, C. W.; Lv, A. Q.; Xie, W.; Shen, K.; Chen, Y. M.; Xie, G. H.; Ma, H. L.; Li, H. B.; Hang, X. C. Tetradentate Pt(II) Complexes with Peripheral Hindrances for Highly Efficient Solution-Processed Blue Phosphorescent OLEDs. *Inorg. Chem.* **2022**, *61* (27), 10402−10409.
(74) Chen, Y. M.; Qian, C. Y.; Qin, K.; Li, H. B.; Shi, X. B.; Lu, Z. Z.; Ma, H. L.; Qin, T. S.; Hang, X. C.; Huang, W. Ultrapure Blue Phosphorescent Organic Light-Emitting Diodes Employing a Twisted Pt(II) Complex. *ACS Appl. Mater. Interfaces* **2021**, *13* (44), 52833−52839.
(75) Li, G. J.; Zhao, X. D.; Fleetham, T.; Chen, Q. D.; Zhan, F.; Zheng, J. B.; Yang, Y. F.; Lou, W. W.; Yang, Y. N.; Fang, K. Tetradentate Platinum(II) Complexes for Highly Efficient Phosphorescent Emitters and Sky Blue OLEDs. *Chem. Mater.* **2020**, *32* (1), 537−548.
(76) Ma, H. L.; Shen, K.; Wu, Y. P.; Xia, F.; Yu, F. L.; Sun, Z. Y.; Qian, C. Y.; Peng, Q. M.; Zhang, H. H.; You, C.; et al. High-color-purity and efficient solution-processable blue phosphorescent light-emitting diodes with Pt(ii) complexes featuring $^3\pi\pi^*$ transitions. *Mater. Chem. Front.* **2019**, *3* (11), 2448−2454.
(77) You, C.; Xia, F.; Zhao, Y.; Zhang, Y.; Sheng, Y. J.; Wu, Y. P.; Hang, X. C.; Chen, F.; Ma, H. L.; Shen, K.; et al. Probing Triplet Excited States and Managing Blue Light Emission of Neutral Tetradentate Platinum(II) Complexes. *J. Phys. Chem. Lett.* **2018**, *9* (9), 2285−2292.
(78) Fleetham, T.; Huang, L.; Li, J. Tetradentate Platinum Complexes for Efficient and Stable Excimer-Based White OLEDs. *Adv. Funct. Mater.* **2014**, *24* (38), 6066−6073.
(79) Li, G.; Ecton, J.; O'brien, B.; Li, J. Efficient and stable red organic light emitting devices from a tetradentate cyclometalated platinum complex. *Org. Electron.* **2014**, *15* (8), 1862−1867.
(80) Becke, A. D. DENSITY-FUNCTIONAL THERMOCHEMISTRY.3. THE ROLE OF EXACT EXCHANGE. *J. Chem. Phys.* **1993**, *98* (7), 5648−5652.
(81) Chai, J. D.; Head-Gordon, M. Long-range corrected hybrid density functionals with damped atom-atom dispersion corrections. *Phys. Chem. Chem. Phys.* **2008**, *10* (44), 6615−6620.
(82) Yanai, T.; Tew, D. P.; Handy, N. C. A new hybrid exchange-correlation functional using the Coulomb-attenuating method (CAM-B3LYP). *Chem. Phys. Lett.* **2004**, *393* (1−3), 51−57.
(83) Yu, H. Y. S.; He, X.; Li, S. H. L.; Truhlar, D. G. MN15: A Kohn-Sham global-hybrid exchange-correlation density functional with broad accuracy for multi-reference and single-reference systems and noncovalent interactions. *Chem. Sci.* **2016**, *7* (8), 5032−5051.
(84) Zhao, Y.; Truhlar, D. G. The M06 suite of density functionals for main group thermochemistry, thermochemical kinetics, noncovalent interactions, excited states, and transition elements: Two new functionals and systematic testing of four M06-class functionals and 12 other functionals. *Theor. Chem. Acc.* **2008**, *120* (1−3), 215−241.
(85) Tao, J.; Perdew, J. P.; Staroverov, V. N.; Scuseria, G. E. Climbing the Density Functional Ladder: Nonempirical Meta−Generalized Gradient Approximation Designed for Molecules and Solids. *Phys. Rev. Lett.* **2003**, *91* (14), 146401.
(86) Staroverov, V. N.; Scuseria, G. E.; Tao, J. M.; Perdew, J. P. Comparative assessment of a new nonempirical density functional: Molecules and hydrogen-bonded complexes. *J. Chem. Phys.* **2003**, *119* (23), 12129−12137.
(87) Boese, A. D.; Martin, J. M. L. Development of density functionals for thermochemical kinetics. *J. Chem. Phys.* **2004**, *121* (8), 3405−3416.
(88) Becke, A. D. A NEW MIXING OF HARTREE-FOCK AND LOCAL DENSITY-FUNCTIONAL THEORIES. *J. Chem. Phys.* **1993**, *98* (2), 1372−1377.
(89) Reiher, M.; Salomon, O.; Hess, B. A. Reparameterization of hybrid functionals based on energy differences of states of different multiplicity. *Theor. Chem. Acc.* **2001**, *107* (1), 48−55.
(90) Adamo, C.; Barone, V. Toward reliable density functional methods without adjustable parameters: The PBE0 model. *J. Chem. Phys.* **1999**, *110* (13), 6158−6170.
(91) Grimme, S.; Hansen, A.; Brandenburg, J. G.; Bannwarth, C. Dispersion-Corrected Mean-Field Electronic Structure Methods. *Chem. Rev.* **2016**, *116* (9), 5105−5154.
(92) Perdew, J. P.; Burke, K.; Ernzerhof, M. Generalized gradient approximation made simple. *Phys. Rev. Lett.* **1996**, *77* (18), 3865−3868.

https://doi.org/10.1021/acs.jpca.4c08452
J. Phys. Chem. A 2025, 129, 2493−2509

(93) Becke, A. D. DENSITY-FUNCTIONAL EXCHANGE-ENERGY APPROXIMATION WITH CORRECT ASYMPTOTIC-BEHAVIOR. *Phys. Rev. A* **1988**, *38* (6), 3098−3100.
(94) Perdew, J. P. DENSITY-FUNCTIONAL APPROXIMATION FOR THE CORRELATION-ENERGY OF THE INHOMOGENEOUS ELECTRON-GAS. *Phys. Rev. B* **1986**, *33* (12), 8822−8824.
(95) Frisch, M. J.; Trucks, G. W.; Schlegel, H. B.; Scuseria, G. E.; Robb, M. A.; Cheeseman, J. R.; Scalmani, G.; Barone, V.; Petersson, G. A.; Nakatsuji, H., et al. *Gaussian 16, revision C.01*; Gaussian, Inc.: Wallingford, CT, 2019.
(96) Weigend, F.; Ahlrichs, R. Balanced basis sets of split valence, triple zeta valence and quadruple zeta valence quality for H to Rn: Design and assessment of accuracy. *Phys. Chem. Chem. Phys.* **2005**, *7* (18), 3297−3305.
(97) Weigend, F. Accurate Coulomb-fitting basis sets for H to Rn. *Phys. Chem. Chem. Phys.* **2006**, *8* (9), 1057−1065.
(98) Tomasi, J.; Mennucci, B.; Cammi, R. Quantum mechanical continuum solvation models. *Chem. Rev.* **2005**, *105* (8), 2999−3093.
(99) Lu, T.; Chen, F. W. Multiwfn: A multifunctional wavefunction analyzer. *J. Comput. Chem.* **2012**, *33* (5), 580−592.
(100) Liu, Z. Y.; Lu, T.; Chen, Q. X. An sp-hybridized all-carboatomic ring, cyclo 18 carbon: Electronic structure, electronic spectrum, and optical nonlinearity. *Carbon* **2020**, *165*, 461−467.
(101) Bousquet, M. H. E.; Papineau, T. V.; Veys, K.; Escudero, D.; Jacquemin, D. Extensive Analysis of the Parameters Influencing Radiative Rates Obtained through Vibronic Calculations. *J. Chem. Theory Comput.* **2023**, *19* (16), 5525−5547.
(102) Sando, G. M.; Spears, K. G. Ab initio computation of the Duschinsky mixing of vibrations and nonlinear effects. *J. Phys. Chem. A* **2001**, *105* (22), 5326−5333.
(103) Cheong, K.; Han, S. W.; Lee, J. Y. Tetradentate Pt(II) Complexes with Bulky Carbazole Moieties for High-Efficiency and Narrow-Emitting Blue Organic Light-Emitting Devices. *Small Methods* **2024**, *8* (10), 2301710.
(104) Cheong, K.; Jo, U.; Hong, W. P.; Lee, J. Y. Fused Cycloalkyl Unit-Functionalized Tetradentate Pt(II) Complexes for Efficient and Narrow-Emitting Deep Blue Organic Light-Emitting Diodes. *Small Methods* **2024**, *8* (3), 2300862.
(105) Fu, T.; Cheng, S.; Chen, Y.; Chang, Y.; Jiao, X.; Zhang, C.; Xia, Q. H.; Sun, Z.; Hang, X. -C. N-Heterocyclic Carbene Based Pt(II) Complexes with d-p Transition for Highly Performable Green Phosphorescent Electroluminescence. *Adv. Opt. Mater.* **2024**, *12* (2), 2301321.
(106) Li, G. J.; Wen, J. F.; Zhan, F.; Lou, W. W.; Yang, Y. F.; Hu, Y.; She, Y. B. Fused 6/5/6 Metallocycle-Based Tetradentate Pt(II) Emitters for Efficient Green Phosphorescent OLEDs. *Inorg. Chem.* **2022**, *61* (29), 11218−11231.
(107) Ferrer, F. J. A.; Santoro, F. Comparison of vertical and adiabatic harmonic approaches for the calculation of the vibrational structure of electronic spectra. *Phys. Chem. Chem. Phys.* **2012**, *14* (39), 13549−13563.
(108) Bloino, J.; Baiardi, A.; Biczysko, M. Aiming at an accurate prediction of vibrational and electronic spectra for medium-to-large molecules: An overview. *Int. J. Quantum Chem.* **2016**, *116* (21), 1543−1574.
(109) Cerezo, J.; Santoro, F. Revisiting Vertical Models To Simulate the Line Shape of Electronic Spectra Adopting Cartesian and Internal Coordinates. *J. Chem. Theory Comput.* **2016**, *12* (10), 4970−4985.
(110) Charaf-Eddin, A.; Planchat, A.; Mennucci, B.; Adamo, C.; Jacquemin, D. Choosing a Functional for Computing Absorption and Fluorescence Band Shapes with TD-DFT. *J. Chem. Theory Comput.* **2013**, *9* (6), 2749−2760.
(111) Latouche, C.; Skouteris, D.; Palazzetti, F.; Barone, V. TD-DFT Benchmark on Inorganic Pt(II) and Ir(III) Complexes. *J. Chem. Theory Comput.* **2015**, *11* (7), 3281−3289.
(112) Vazart, F.; Latouche, C.; Bloino, J.; Barone, V. Vibronic Coupling Investigation to Compute Phosphorescence Spectra of Pt(II) Complexes. *Inorg. Chem.* **2015**, *54* (11), 5588−5595.

https://doi.org/10.1021/acs.jpca.4c08452
J. Phys. Chem. A 2025, 129, 2493−2509